

Article

Nanobody therapy rescues behavioural deficits of NMDA receptor hypofunction

<https://doi.org/10.1038/s41586-025-09265-8>

Received: 9 November 2023

Accepted: 10 June 2025

Published online: 23 July 2025

Open access

 Check for updates

Mathieu Oosterlaken^{1,8}, Angelina Rogliardo^{1,6,8}, Tatiana Lipina^{2,8}, Pierre-André Lafon^{1,8}, Mireille Elodie Tsitokana¹, Mathilde Keck³, Hélène Cahuzac³, Pierre Prieu-Sérandon¹, Séverine Diem¹, Cécile Derieux¹, Célia Camberlin¹, Chrystel Lafont¹, Damien Meyer⁴, Patrick Chames⁴, Franck Vandermoere^{1,7}, Philippe Marin¹, Laurent Prézeau¹, Denis Servent³, Ali Salahpour², Amy J. Ramsey², Carine Bécamel¹, Jean-Philippe Pin^{1,9}✉, Julie Kniazeff^{1,5,9}✉ & Philippe Rondard^{1,9}✉

There is an urgent need for efficient and innovative therapies to treat brain disorders such as psychiatric and neurodegenerative diseases. Immunotherapies have proved to be efficient in many medical areas, but have not been considered to treat brain diseases due to the poor brain penetration of immunoglobulins^{1,2}. Here we developed a bivalent biparatopic antibody, made of two camelid heavy-chain antibodies (called nanobodies)³, one binding to, and the other potentiating the activity of, homodimeric metabotropic glutamate receptor 2. We show that this bivalent nanobody, given peripherally, reaches the brain and corrects cognitive deficits in two preclinical mouse models with endophenotypes resulting from NMDA receptor hypofunction. Notably, these *in vivo* effects last for at least 7 days after a single intraperitoneal injection and are maintained after subchronic treatment. Our results establish a proof of concept that nanobodies can target brain receptors, and pave the way for nanobody-based therapeutic strategies for the treatment of brain disorders.

The majority of brain diseases are still in need of new therapies. To date, mostly small molecules are used and developed for these pathologies, but they sometimes lack selectivity and/or show off-target binding resulting in side effects. Alternatively, antibodies are highly specific for their target, but the brain penetration of immunoglobulins (IgGs) is rather limited^{1,2}, such that immunotherapy for brain diseases has seldomly been considered. However, recent efforts to develop innovative treatments for Alzheimer's diseases highlight the possibility of using antibodies to target the brain^{4,5}. Nanobodies, which are variable V_{HH} domains of the camelid heavy-chain antibodies and the smallest proteins derived from the immune system³, could be envisioned as an alternative to target brain diseases. With a molecular mass of 15 kDa and only three complementarity-determining regions, they are able to bind to small cavities of their protein target and stabilize specific conformations to modulate target activity³. Although it is commonly assumed that nanobodies cannot reach the brain, a few have shown brain-penetration abilities^{6–9}, raising the possibility that some nanobodies could be used to treat brain pathologies¹⁰.

Over the past decade, an increasing number of nanobodies targeting and modulating cell surface receptors have been reported with a wide range of pharmacological profiles including allosteric modulations^{11–15}. As derivatives of the immune system, these allosteric modulator nanobodies are hydrophilic and highly selective for their target. Moreover, when acting as allosteric modulators of receptor function, they preserve

temporal and spatial patterns of physiological activation. As such, positive modulator nanobodies are less prone to inducing side effects, in contrast to small-molecule hydrophobic modulators. They represent an alternative to small molecules for controlling the activity of cell surface receptors, including those involved in synaptic transmission¹⁶. Notably, we previously reported DN13—a nanobody that functions as a positive allosteric modulator (PAM) specific for the metabotropic glutamate 2 (mGlu2) receptor homodimer¹¹, which is considered a target to reduce glutamatergic tone in brain regions related to schizophrenia^{17,18}. Indeed, several drugs targeting mGlu2 in schizophrenia have been developed and validated in phase II clinical trials^{19–21}. However, they failed in phase III trials for multiple reasons, including action on the mGlu3 receptor and decreased mGlu2 expression in patients treated with antipsychotics²². Notably, DN13 binds to only the agonist-bound conformation of the large extracellular domain of the mGlu2 homodimer, with no binding to other mGlu receptors^{11,23}. Moreover, the PAM property of DN13 was confirmed for endogenous mGlu2 receptors both *ex vivo* on brain slices and *in vivo* in a fear-conditioning paradigm after direct injection into the brain¹¹. Consequently, DN13 appears to be a good candidate to determine whether a nanobody can be used to decrease symptoms associated with a brain disorder and whether peripheral administration leads to central behavioural effects.

Here we establish the proof of concept that an optimized nanobody potentiating the mGlu2 receptor penetrates the brain after peripheral

¹Institut de Génomique Fonctionnelle, Université de Montpellier, CNRS, INSERM, Montpellier, France. ²Department of Pharmacology & Toxicology, University of Toronto, Toronto, Ontario, Canada.

³Département Médicaments et Technologies pour la Santé (DMTS), SIMoS, Université Paris Saclay, CEA, Gif-sur-Yvette, France. ⁴Institute Paoli-Calmettes, CCRM, Aix Marseille University, CNRS, INSERM, Marseille, France. ⁵Institut des Biomolécules Max Mousseron, Université de Montpellier, CNRS, ENSCM, Montpellier, France. ⁶Present address: Institut des Neurosciences de Montpellier, Montpellier, France. ⁷Present address: Institute Paoli-Calmettes, CCRM, Aix Marseille University, CNRS, INSERM, Marseille, France. ⁸These authors contributed equally: Mathieu Oosterlaken, Angelina Rogliardo, Tatiana Lipina, Pierre-André Lafon. ⁹These authors jointly supervised this work: Jean-Philippe Pin, Julie Kniazeff and Philippe Rondard. [✉]e-mail: jean-philippe.pin@igf.cnrs.fr; julie.kniazeff@cnrs.fr; philippe.rondard@igf.cnrs.fr

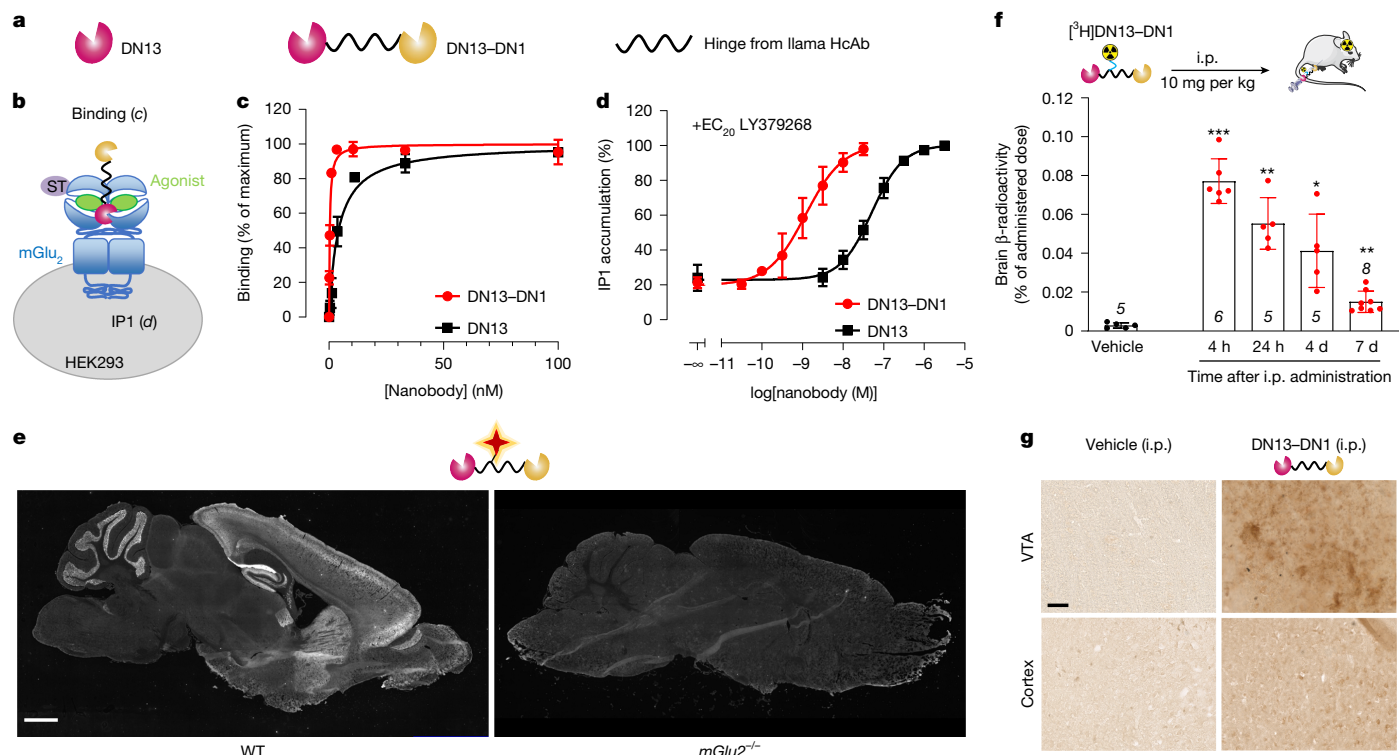


Fig. 1 | The mGlu2-specific DN13-DN1 nanobody potentiates receptor activation and penetrates the brain. **a**, Schematic of DN13 and the bivalent biparatopic DN13-DN1 in which the two nanobodies are linked using the hinge from llama heavy-chain antibodies (HcAb). **b**, Cartoon of the mGlu2 receptor fused to an extracellular SNAP tag (ST) for labelling and the 6×His-tagged DN13-DN1 binding to the receptor. Intracellular IP1 accumulation is a functional readout of mGlu2 receptor activation. **c**, Saturation binding experiments of DN13 and DN13-DN1 on cells expressing SNAP-mGlu2 in the presence of a saturating concentration of the agonist LY379268 (1 μM). Data are mean ± s.d. of three individual experiments each performed in quadruples. **d**, Potentiation of IP1 accumulation induced by the indicated nanobodies in the presence of LY379268 (EC₂₀, 0.6 nM). Data are mean ± s.d. of three individual experiments each performed in triplicates. **e**, Ex vivo immunofluorescence analysis of brain sagittal sections from WT (left) or *mGlu2*^{-/-} (right) mice using

d2-labelled DN13-DN1. Scale bar, 1.1 mm. White levels were modified uniformly (Zen, Zeiss). Representative slices of two technical replicates from three animals. **f**, Quantification of the radioactivity present in the mouse brain 4 h, 24 h, 4 days or 7 days after i.p. administration of [³H]DN13-DN1. Data are mean ± s.d. of the indicated number of animals (*n*). Statistical analysis was performed using Brown–Forsythe and Welch analysis of variance (ANOVA) with Dunnett’s multiple-comparison test compared with the vehicle treatment; **P*<0.05, ***P*<0.01, ****P*<0.001. **g**, Immunohistochemical detection of DN13-DN1 in the ventral tegmental area (VTA) (top) and in the cerebral cortex (bottom) 24 h after i.p. administration of DN13-DN1 (right) versus vehicle (left). Representative slices of four technical replicates from two animals. Scale bar, 50 μm. The diagram in **f** was partly generated using Servier Medical Art, provided by Servier, under a CC BY 4.0 license.

administration and corrects behavioural deficits resulting from NMDA receptor hypofunction. Such effects were observed in two preclinical models, one resulting from NMDA receptor inhibition with phenylclidine early during development²⁴, while the second mimics a rare human disease (GRIN1 disorder) that results from a low expression of the GluN1 subunit^{25,26}. Notably, the nanobody still improves cognition and sensorimotor gating 7 days after a single peripheral injection, and also after subchronic treatment. Together, our observations open perspectives for nanobody-based immunotherapies for brain diseases.

A bivalent nanobody potentiates mGlu2 receptor

To increase the likelihood of observing a pharmacological effect in the brain even at a low nanobody concentration, our rationale was to improve the affinity of the mGlu2 PAM nanobody DN13 that we already developed¹¹. We generated and screened a number of bivalent nanobodies using two different linkers to fuse DN13 to the mGlu2 selective neutral DN1 or to the agonist-PAM DN10 (Fig. 1a,b and Extended Data Fig. 1). This is a well-known strategy to increase the avidity or the residence time of a nanobody on its target or both. We selected the bivalent biparatopic DN13-DN1 (Fig. 1a) that showed a tenfold increase in the apparent affinity (*K*_d) for mGlu2 compared with DN13 alone (0.50 nM (*pK*_d=9.30±0.25) and 4.10 nM (*pK*_d=8.39±0.30), respectively) in the

presence of agonist (LY379268 1 μM; Fig. 1c and Extended Data Fig. 2a). Moreover, we detected an almost 2-log increase in PAM potency for DN13-DN1 (half-maximum effective concentration (EC₅₀)=1.76 nM; negative logarithm of the EC₅₀ (*pEC*₅₀)=8.75±0.40) compared with DN13 (EC₅₀=101 nM; *pEC*₅₀=7.00±0.33) to enhance mGlu2 activation by agonist LY379268 (Fig. 1d) and glutamate (Extended Data Figs. 1c and 2b).

Like DN13 and DN1¹¹, DN13-DN1 is specific for mGlu2 over the other mGlu receptors (Extended Data Fig. 1d). The specificity of DN13-DN1 for mGlu2 in the brain was validated by ex vivo immunohistofluorescence analysis using a far-red d2-labelled DN13-DN1 that preserved its binding properties (Fig. 1e and Extended Data Fig. 1e). Sagittal brain sections from wild-type (WT) C57BL/6J mice revealed mGlu2 labelling in regions that are known to express this receptor, including the prefrontal cortex, the hippocampus, the striatum, the cerebellum and the olfactory bulb²⁷. No labelling was detected in brain tissue sections from *mGlu2*^{-/-} mice (Fig. 1e).

DN13-DN1 reaches the brain

To assess the suitability of the intraperitoneal (i.p.) route to administer the nanobody in a similar manner to small molecules, we first evaluated the pharmacokinetic profile of DN13-DN1 and DN13 in the blood stream, as they might be quickly eliminated by the kidney due to their small size²⁸. We developed a time-resolved FRET-based assay (Extended

Data Fig. 3a–e) to quantify the amount of nanobodies in blood samples collected at different times after i.p. administration of 10 mg per kg of nanobodies. Elimination of DN13–DN1 was significantly slower than the smaller-sized DN13, and DN13–DN1 was detected for about 8 h.

A fraction of the administered DN13–DN1 penetrated the brain (Fig. 1f,g), as previously reported for a few other nanobodies^{6–8}. To determine this, we labelled DN13–DN1 with tritium on a single lysine residue using bacterial transglutaminase and the CBz-Gln-Gly-Lys(³H)Pr-OH peptide, a derivatization strategy that preserved the binding properties on the mGlu2 receptor (Extended Data Fig. 1f). After a 10 mg per kg i.p. administration, [³H]DN13–DN1 levels reached their maximum at 4 h after administration, with 0.08% of the administered radioactivity detected in the total brain extracts. Radioactivity was still detected up to 7 days after injection in mice (Fig. 1f). Considering a homogenous nanobody distribution in the whole brain volume (about 500 mm³), we estimated that the DN13–DN1 brain concentration reaches 9.2 nM at 4 h after administration, which is about 20× the K_d , and reduces to 1.5 nM 7 days after administration, which is still over 3× the K_d . The local concentration could be even higher near mGlu2-expressing neurons as they would trap the circulating nanobody due to the DN1 domain, therefore limiting the diffusion and potentially leading to a non-homogenous distribution. For a more qualitative analysis of the DN13–DN1 brain distribution, we used immunohistochemistry. At 24 h after DN13–DN1 i.p. administration (10 mg per kg) in mice, brains were fixed and brain sections were labelled using an antibody recognizing the 6×His tag of DN13–DN1. DN13–DN1 was detected in various brain region such as the ventral tegmental area or in the cortex (Fig. 1g and Extended Data Fig. 3f). No immunoreactivity was detected in the brain of vehicle-injected mice (Fig. 1g and Extended Data Fig. 3f). The cortical localization of the nanobody was also confirmed by autoradiography on brain slices of [³H]DN13–DN1-treated mice 24 h after i.p. administration (Extended Data Fig. 3g). Together, these observations indicate that DN13–DN1 penetrates the brain sufficiently to potentiate mGlu2, concentrates in some brain areas and remains present for up to 7 days.

DN13–DN1 improves recognition memory

To assess the efficacy of DN13–DN1 *in vivo*, we used a neonatal phenylclidine (PCP) mouse model that recapitulates in adult animals cognitive and other behavioural changes resulting from NMDA receptor hypofunction, and characteristic of schizophrenia²⁴. In this model, administration of the NMDA receptor antagonist PCP, at postnatal days 7, 9 and 11, induces cognitive deficits that can be measured in adulthood using the novel-object recognition (NOR) test (Fig. 2a,b). We first found that intracerebroventricular (i.c.v.) injection of DN13–DN1 directly into the brain (4 pmol in 5 µl) restores a normal cognitive performance in NOR in PCP-treated mice with a 24 h retention interval (Fig. 2c). This approach enables precise control of the nanobody quantity delivered into the brain (>15 × K_d). The DN13–DN1 effect was similar to that obtained with the mGlu2/mGlu3 orthosteric agonist LY379268 (1 mg per kg, i.p.). By contrast, the mGlu2-selective neutral DN1 nanobody at the same dose (4 pmol in 5 µl) did not ameliorate the discrimination index for NOR in PCP-treated mice, confirming the importance of DN13–DN1 PAM property to observe a behavioural effect. Moreover, we determined that neither DN13–DN1 nor DN1 or LY379268 altered the cognitive performance in control vehicle-treated mice in the NOR task (Extended Data Fig. 4a). Notably, DN13–DN1 was injected only once 24 h before the NOR training phases, that is, 48 h before the NOR test, while LY379268 was injected twice, 1 h before the training and 1 h before the NOR test performed the next day (Fig. 2c). Together, these data indicate that a single administration of DN13–DN1 into the brain 2 days before the behavioural experiment is as efficient as an acute administration of the orthosteric mGlu2/mGlu3 agonist to improve cognitive function in this model.

When administered i.p. (10 mg per kg), DN13–DN1 also restored the cognitive capacity of PCP-treated mice, in agreement with its brain

penetration. Indeed, the discrimination index of PCP-treated mice in NOR was similar to that obtained after LY379268 administration or i.c.v. administration of DN13–DN1 (Fig. 2c). Importantly, the beneficial effect of DN13–DN1 was completely inhibited by the injection of the mGlu2/mGlu3 antagonist LY341495 (3 mg per kg) administered 30 min before the injection of the nanobody (Fig. 2c). We also confirmed that the observed behavioural effect was not linked to changes in locomotion (Extended Data Fig. 5a,b), changes in mGlu2 receptor expression (Extended Data Fig. 6a,b) and that there was no sex difference (Extended Data Fig. 7a). Importantly, we show that DN13–DN1 still improves cognitive performance 7 days after i.p. administration while the small-molecule agonist LY379268 had no longer an effect, as assessed in the NOR test with a 7-day-retention period (Fig. 2d and Extended Data Fig. 4b). This indicates that DN13–DN1 modulates brain mGlu2 receptor activity and maintains an improved cognitive performance up to 7 days after a single peripheral administration, while small molecules do not.

DN13–DN1 restores working memory and sensory gating

To confirm the DN13–DN1 behavioural effect in another model of NMDA receptor hypofunction, we used the GluN1-knockdown (GluN1 KD) genetic mouse model that mimics the rare human genetic disease GRIN1^{25,26}. GluN1-KD mice have a hypomorphic mutation of *Grin1* that leads to a partial loss-of-function due to the reduction in the amount of GluN1 containing NMDA receptors uniformly in the brain. The behavioural profile of GluN1-KD mice resembled that of mice treated with low doses of NMDA receptor antagonist, as previously reported²⁵. GluN1-KD mice displayed impairments in performance in the Y-maze behavioural test, which assesses short-term working memory (Fig. 3a,b). Notably, a single i.p. administration of DN13–DN1 (20 mg per kg) markedly improved working memory 3 h after injection. The effect was similar to that induced by LY379268 (1 mg per kg) injected 1 h before the test. The increased alternations were not due to a drug- or nanobody-induced augmentation of the GluN1-KD mouse hyperactivity (Extended Data Figs. 4c,d and 5c,d). As a control, we verified that neither DN13–DN1 nor LY379268 had an effect on WT mice treated under the same conditions (Fig. 3b). Notably, 7 days after administration, DN13–DN1 still improved the working memory of GluN1-KD mice, while the mice treated with the agonist LY379268 no longer showed an effect (Fig. 3c and Extended Data Fig. 4e). These results show that DN13–DN1 improves short-term working memory in the GluN1-KD mice for at least 7 days, an effect that results from its ability to reach and remain in the brain for up to 7 days, potentiating the mGlu2 receptor activity.

GluN1-KD mice also display deficiency in sensory processing^{29–31}. Sensorimotor gating was evaluated using pre-pulse inhibition (PPI) of the acoustic startle response. As previously reported^{29–31}, the gating was impaired in the GluN1-KD mice (Fig. 3d–f and Extended Data Fig. 4f–h). The impairment was reduced when GluN1-KD mice were treated with a single i.p. injection of DN13–DN1 (20 mg per kg), an effect observed 3 h after nanobody administration for an 81 dB prepulse intensity (Fig. 3e). Notably, and reminiscent of our observations in the Y-maze test and in NOR test in PCP-treated mice, retesting the animals 7 days later without additional compound administration showed that DN13–DN1 was still efficient at restoring the PPI of GluN1-KD mice. Indeed, the nanobody effect was even stronger at 7 days, as a decreased startle response was seen for both 69 dB and 81 dB prepulse intensities (Fig. 3f). WT and vehicle-treated mice showed a similar response in both test days, indicating that the mice did not show habituation due to the former experiment. Moreover, on the first testing day, the effect of DN13–DN1 was similar to that of the agonist LY379268 injected 1 h before the test (Fig. 3e); however, 7 days later, without further administration of LY379268, only the group treated with DN13–DN1 showed an improved response (Fig. 3f). DN13–DN1 treatment did not modify mGlu2 receptor

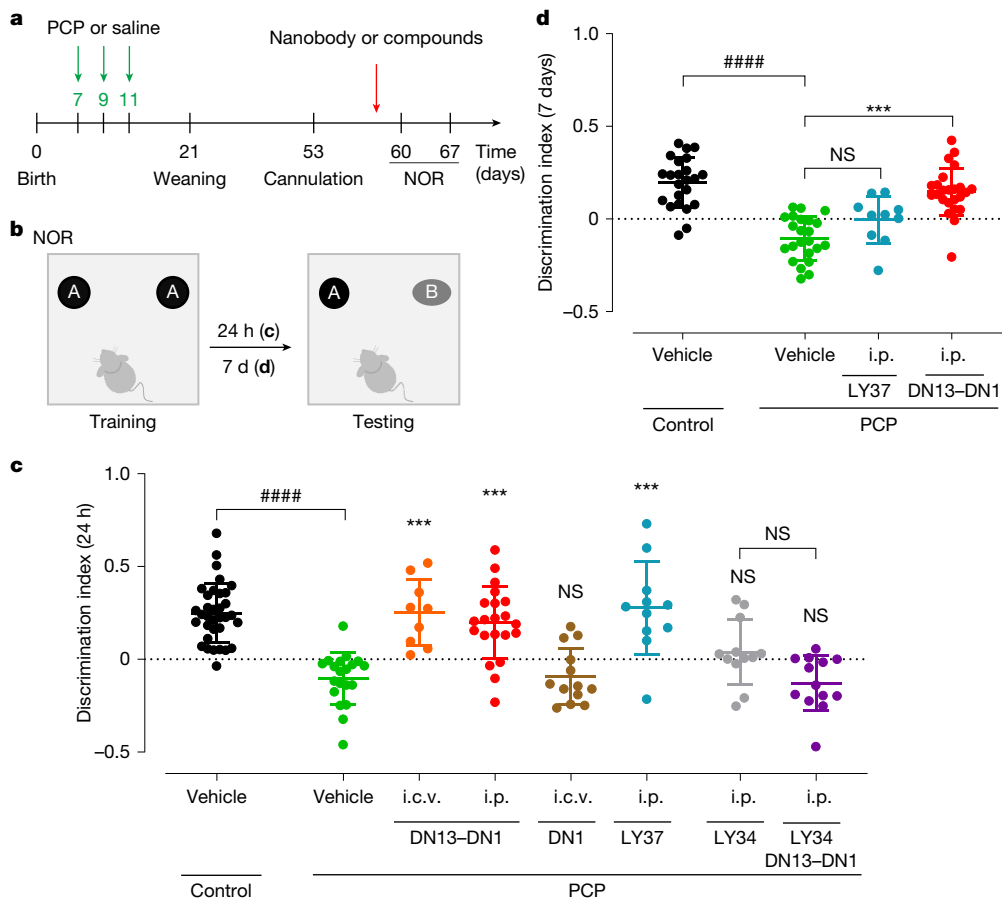


Fig. 2 | DN13-DN1 nanobody rescues recognition memory in a neurodevelopmental PCP-induced mouse model of schizophrenia.

a, Schematic of the experimental timeline. **b**, Schematic of the NOR protocol with either a 24 h or 7 day retention period between the training and testing phases (for **c** and **d**, respectively). **c**, The discrimination index was determined using the NOR task 24 h after training in control ($n = 34$) or PCP-treated ($n = 20$) mice additionally treated with vehicle, and in PCP-treated animals additionally treated with DN13-DN1 i.c.v. (4 pmol, 5 μ l; 48 h after administration; orange; $n = 9$) or i.p. (10 mg per kg; 24 h after administration; red; $n = 21$), the negative control DN1 (4 pmol, 5 μ l i.c.v.; brown; $n = 13$) and the reference mGlu2 agonist (LY379268; 1 mg per kg i.p.; 1 h after the second administration; blue; $n = 11$). The effect of the mGlu2 antagonist LY341495

(3 mg per kg i.p.) alone (grey; $n = 12$) or with DN13-DN1 (purple; $n = 13$) was tested. **d**, The discrimination index was determined using the NOR task 7 days after training in mice treated with DN13-DN1 i.p. (10 mg per kg; red; $n = 24$) and LY379268 (1 mg per kg i.p.; blue; $n = 10$) compared with mice treated with vehicle and PCP (green; $n = 23$) and mice treated with vehicle control (black; $n = 23$). For **c** and **d**, data are mean \pm s.d. Statistical analysis was performed using one-way ANOVA followed by Dunnett's multiple-comparison test compared with the control mice (black; hash symbols), or compared with the PCP-treated mice (green) or the indicated groups (all other comparisons). NS, not significant. **** $P < 0.0001$, *** $P < 0.001$. Details on statistics and P values are provided as source data.

expression in various brain areas (Extended Data Fig. 6c) and the observed behavioural effect is not linked to the sex (Extended Data Fig. 7d) or the weight of the animals (Extended Data Fig. 8a,b). Taken together these results show that the bivalent nanobody DN13-DN1 has a long-lasting effect in improving the cognitive deficits and sensorimotor gating impairments of the GluN1-KD mice, after a single i.p. administration, while the effect of small molecules is more transient.

Lack of behavioural effect of a larger antibody

We next examined whether an IgG-like format would show similar behavioural improvements as nanobodies. To our knowledge there are no mGlu2 IgGs that increase the receptor activity. We therefore generated a DN13-Fc construct corresponding to the fusion of two DN13 nanobodies to a Fc domain of human IgG1 leading to an 80 kDa protein (Fig. 4a). As expected, DN13-Fc binds to and exerts a PAM effect on mouse mGlu2 receptors (Extended Data Fig. 2).

In contrast to DN13-DN1 (10 mg per kg i.p.), acute i.p. administration of DN13-Fc (10 mg per kg) does not improve behavioural impairment in the neurodevelopmental PCP mouse model (Fig. 4b and Extended

Data Fig. 9a) or in the genetic mouse model (Fig. 4c,d and Extended Data Fig. 9b) regardless of the sex of the animals (Extended Data Fig. 7b,d). Moreover, the hyperlocomotion of GluN1-KD mice is significantly reduced by DN13-DN1, while DN13-Fc has no effect on locomotor activity as assessed in an open-field test (Extended Data Fig. 5c,d). These results show that a dose of 10 mg per kg of DN13-DN1 is sufficient to obtain behavioural improvements in GluN1 KD. Importantly, it shows that the nanobody is superior to IgG-like antibodies to target brain mGlu2 receptors and correct associated brain deficits.

For these studies, DN13-DN1 was produced in bacteria, which may result in contamination by endotoxins and, therefore, inflammation and side effects in animal after administration. Visual observation of the animals did not reveal any notable effect of the nanobody. Moreover, we performed a series of experiments showing no effect of 10 mg per kg DN13-DN1 on motor coordination, balance and cataleptic behaviour in C57BL/6J mice (Extended Data Fig. 8c). To further exclude that the positive behavioural effects of DN13-DN1 is related to endotoxin contamination (24.15 ± 7.55 μ g lipopolysaccharide (LPS) per mg DN13-DN1), we performed additional purification steps to reach an almost endotoxin-free sample (0.19 ± 0.18 μ g LPS per mg DN13-DN1). Notably,

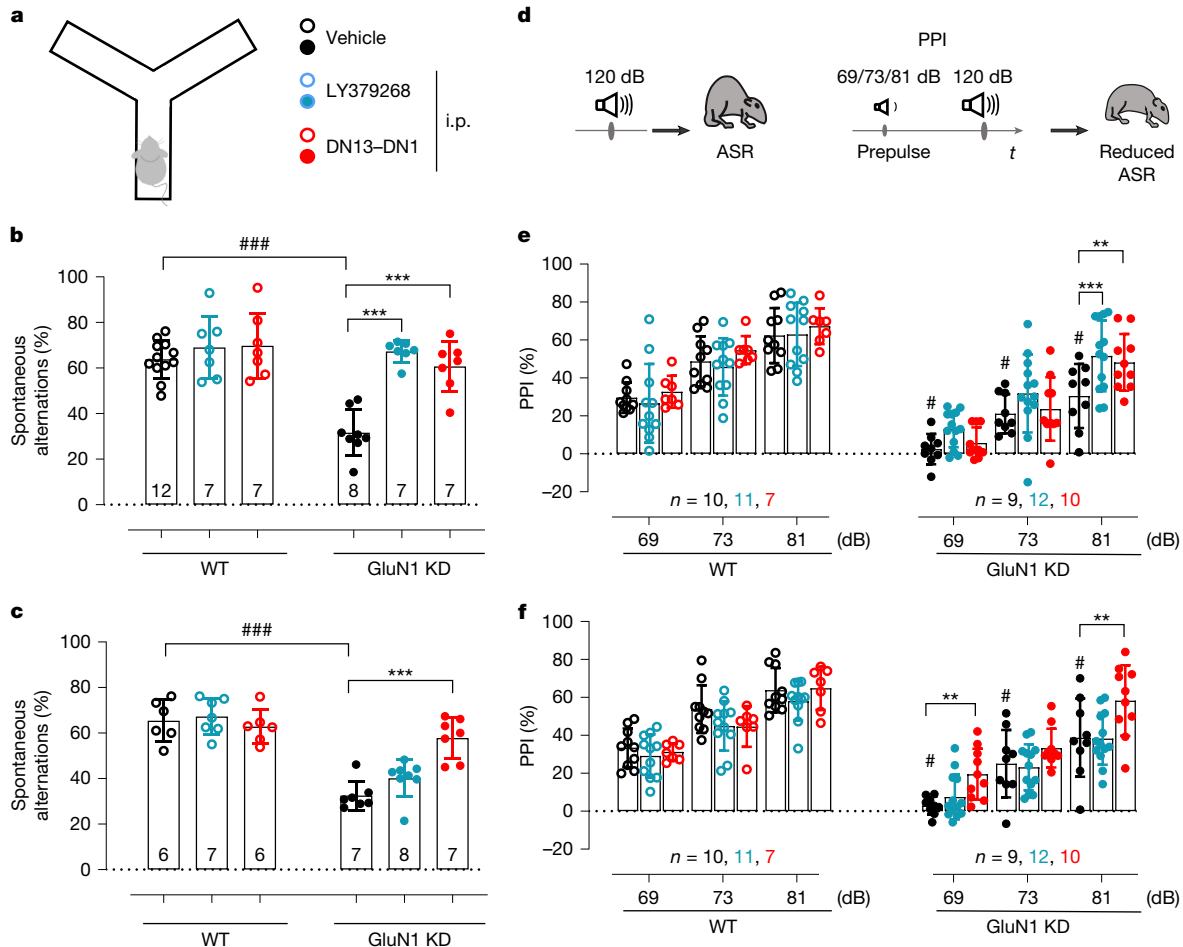


Fig. 3 | DN13-DN1 nanobody improves working memory and sensory gating of GluN1-KD mice. **a–c**, Y-maze experiment. **a**, Schematic of the experiment. Two independent cohorts of mice were used in the Y-maze to examine the effect of drugs at 3 h (**b**) and 7 days (**c**) after acute injection. The colour key in **a** applies to **b**, **c**, **e** and **f**. **b**, **c** The percentage of spontaneous alternations 3 h (**b**) or 7 days (**c**) after treatment in vehicle-treated (black), LY379268-treated (blue) and DN13-DN1-treated (red) mice. None of the studied drugs affected the ambulation of the experimental mice (Extended Data Fig. 4c–e (number of entries)). Data are mean \pm s.d. The number of animals is indicated at the bottom of the bar. Statistical analysis was performed using two-way multivariate ANOVA (MANOVA) followed by Tukey's honest significant difference (HSD) test compared with vehicle-treated WT mice (hash symbols) and compared with vehicle-treated GluN1-KD mice (asterisks); $^{###}P < 0.0001$, $^{***}P < 0.001$.

d–f, The PPI experiment. **d**, Schematic of the experiment. One cohort of mice was tested in PPI at 3 h after drug treatment (**e**) and retested after 7 days (**f**). **e**, **f**, The percentage of PPI was determined in vehicle-treated (black), LY379268-treated (blue) and DN13-DN1-treated (red) mice, assessed 3 h (**e**) or 7 days (**f**) after treatment. DN13-DN1 had no effect on the acoustic startle response (ASR; Extended Data Fig. 4f–h). Data are mean \pm s.d. The number of animals is indicated above the x axis. Statistical analysis was performed using three-way repeated-measures MANOVA (rm-MANOVA) followed by Tukey's HSD test compared with vehicle-treated WT mice (hash symbols) and compared with vehicle-treated GluN1-KD mice (asterisks); $^{\#}P < 0.0001$, $^{**}P < 0.01$, $^{***}P < 0.001$. Details of the statistical analysis and P values are provided as source data.

the corresponding dose of LPS in animals injected with 10 mg per kg of nanobody is either 0.24 ± 0.07 mg or 0.002 ± 0.002 mg (additionally purified sample) (Extended Data Fig. 10a), which are both below the concentrations reported to alter blood–brain barrier integrity or induce neurotoxicity^{32,33}. Importantly, there is no difference between the two preparations of DN13-DN1 (the original and additionally purified) when assessing improvement in working memory in a Y-maze test of GluN1-KD mice (Extended Data Fig. 10b). Together, this confirms that endotoxins are not responsible for brain penetration of DN13-DN1 or positive behavioural effects.

Positive effects maintained after subchronic treatment

After establishing the proof of concept that i.p. administrated mGlu2 nanobody corrects deficits resulting from NMDA receptor hypofunction in two mouse models, we examined whether the benefits were

maintained with a subchronic administration protocol. We administered an initial dose of 10 mg per kg i.p., followed by three doses of 1 mg per kg i.p. DN13-DN1 with a 1 week interval in the neurodevelopmental PCP model and in the genetic GluN1-KD model (Fig. 5a). In this protocol, subchronic DN13-DN1 dosing improved recognition memory (Fig. 5b), working memory (Fig. 5c and Extended Data Fig. 9c) and sensory gating (Fig. 5d and Extended Data Fig. 9c) independent of the sex (Extended Data Fig. 7c,e) or the weight (Extended Data Fig. 8a,b) of the animals. Subchronic DN13-DN1 dosing also reduced GluN1-KD hyperlocomotion (Extended Data Fig. 5e,f).

Changes in receptor expression level are often observed after a long and repeated activation. Notably, subchronic DN13-DN1 administration did not change the mGlu2 expression level in the brain areas that were tested in both animal models (Extended Data Fig. 11). This indicates that nanobody treatment does not promote downregulation of the receptor expression and would therefore be compatible for repeated dosing. Moreover, no toxicity was detected by visual observation of the animals

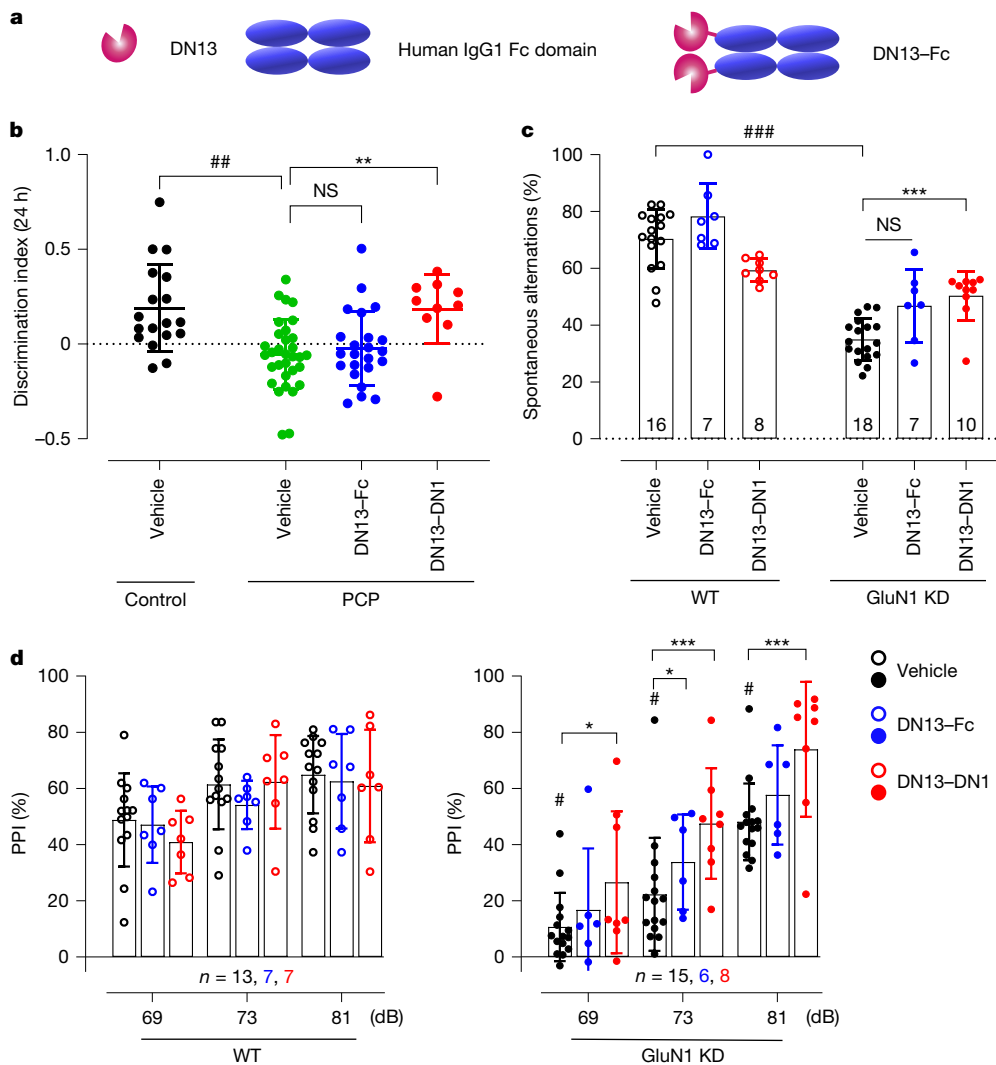


Fig. 4 | Absence of acute behavioural effects of DN13-Fc in the two mouse models of schizophrenia. **a**, Schematic of DN13-Fc, which is a fusion of two DN13 nanobodies to the human IgG1 Fc domain. **b**, The discrimination index was determined using the NOR task 24 h after training in vehicle control mice (black; $n=18$) or in PCP-treated mice that were additionally treated with vehicle (green; $n=32$), DN13-Fc (10 mg per kg, i.p.; 24 h after administration; blue; $n=23$) and DN13-DN1 (10 mg per kg, i.p.; 24 h after administration; red; $n=10$). Data are mean \pm s.d. Statistical analysis was performed using Kruskal–Wallis tests followed by Dunn's multiple-comparison test compared with the control mice (hash symbols) or compared with the other groups (other comparisons); $\#\#P < 0.01$, $**P < 0.01$. **c**, The percentage of spontaneous alternations 3 h after treatment in vehicle-treated (black), DN13-Fc-treated (blue) and

DN13-DN1-treated (red) WT and GluN1-KD mice. Data are mean \pm s.d. The number of animals is indicated at the bottom of the bar. Statistical analysis was performed using two-way MANOVA followed by Tukey's HSD test compared with vehicle-treated WT mice (hash symbols) and compared with vehicle-treated GluN1-KD mice (asterisks); $###P \leq 0.001$, $***P < 0.001$. **d**, The percentage of PPI was assessed 3 h after i.p. injection of vehicle-treated (black), DN13-Fc-treated (blue) and DN13-DN1-treated (red) mice. Data are mean \pm s.d. The number of animals is indicated above the x axis. Statistical analysis was performed using three-way rm-MANOVA followed by Tukey's HSD test compared with vehicle-treated WT mice (hash symbols) and compared with vehicle-treated GluN1-KD mice (asterisks); $\#P < 0.05$, $*P < 0.05$, $**P < 0.001$. Details of the statistical analysis and P values are provided as source data.

after subchronic administration of DN13-DN1 and locomotion of WT mice was also not altered (Extended Data Fig. 5e,f). Taken together, these data indicate that DN13-DN1 may be a promising candidate for further translational studies.

Discussion

Here we describe an optimized bivalent biparatopic nanobody potentiating mGlu2 and show that it reaches the brain and restores cognition and sensorimotor gating in two mouse-models of NMDA receptor hypofunction leading to schizophrenia-like symptoms. This nanobody penetrates the brain during the first hours after i.p. injection and has a long-lasting residency in the brain, up to 7 days. Restoration of behavioural deficits is observed after both acute and

subchronic administration protocols, with an absence of side effects on measures such as locomotion and on visual observation of animals. Importantly, this study reveals the advantage of the nanobody format over small-molecule drugs that are known to have short-term effects. Our data also show the value of nanobodies compared with larger antibody fragments that show no behavioural-improvement effects. Such a long-lasting action of nanobodies could be particularly relevant in therapeutic interventions.

We show here that, although only 0.1% of DN13-DN1 injected i.p. reaches the brain after 4 h, the levels are sufficient to exert beneficial behavioural effects for up to 7 days. Although the percentage of the bivalent DN13-DN1 nanobodies entering the brain is similar to that reported for brain entry of IgGs^{1,2}, IgGs stay in the peripheral circulation for few days or more, in contrast to nanobodies, which are rapidly

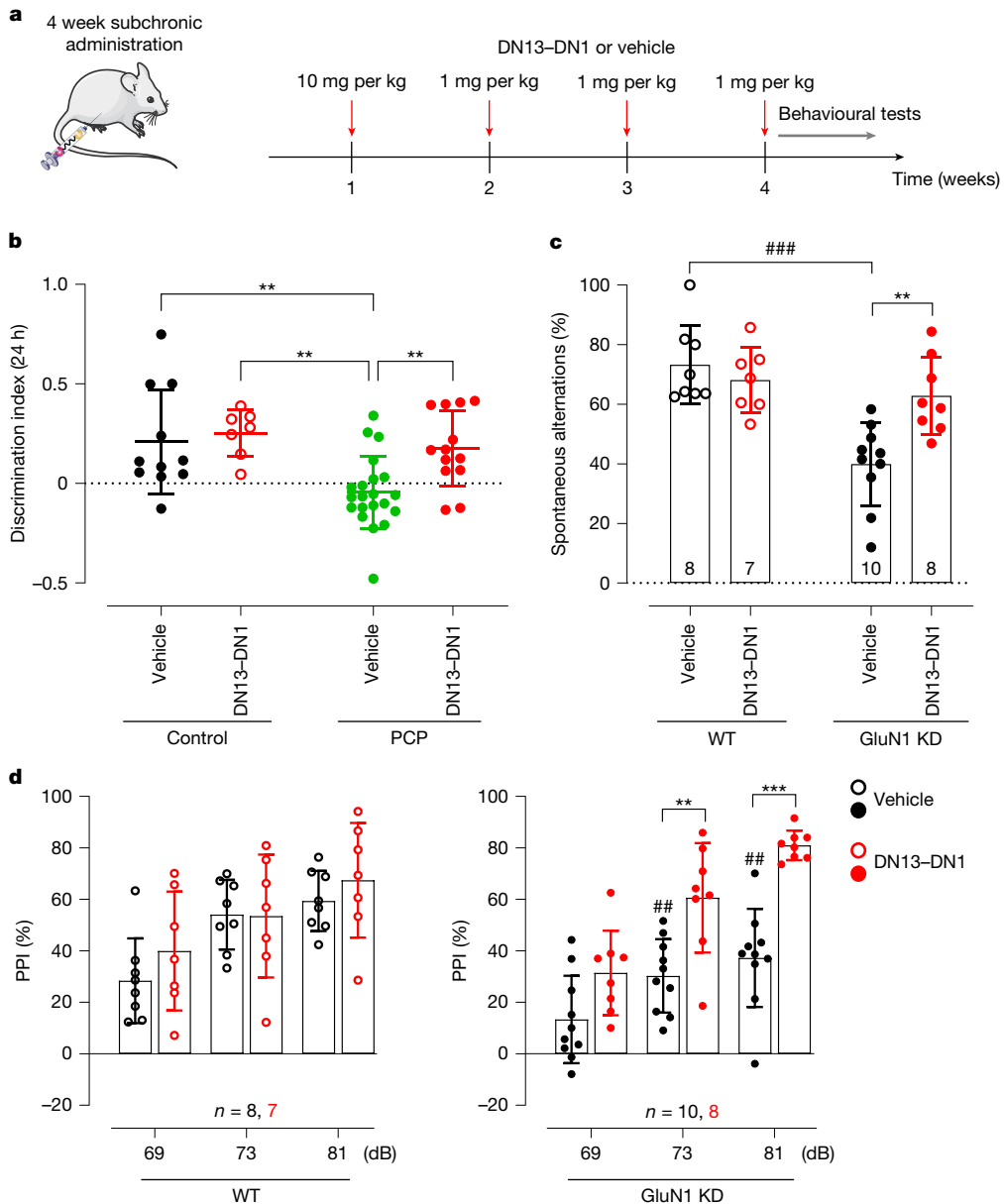


Fig. 5 | Subchronic DN13-DN1 treatment restores behavioural deficits in the two mouse models of schizophrenia. **a**, The timeline of the 4-week subchronic DN13-DN1 administration protocol. After an initial dose of 10 mg per kg i.p., three additional administrations at 1 mg per kg i.p. were performed 1 week apart. **b**, The discrimination index in the NOR task performed 24 h after training in vehicle-treated (black; $n = 11$) or DN13-DN1-treated (red; $n = 7$) control mice, and in vehicle-treated (green; $n = 21$) or DN13-DN1-treated (red; $n = 13$) PCP-treated mice 2 days after the last injection. Data are mean \pm s.d. Statistical analysis was performed using one-way ANOVA followed by Dunnett's multiple-comparison test compared with PCP-treated mice (bottom); $^{**}P < 0.01$ compared with PCP-treated mice. **c**, The percentage of spontaneous alternations was assessed using the Y-maze, 3 h after the last injection of the subchronic treatment in vehicle-treated (black) and DN13-DN1-treated (red) WT and GluN1-KD mice. Data are mean \pm s.d. The number of animals is indicated at the bottom of the bar. Statistical analysis was performed using two-way MANOVA followed by Tukey's HSD test compared with vehicle-treated WT mice (hash symbols) and compared with vehicle-treated GluN1-KD mice (asterisks); $^{###}P < 0.001$, $^{**}P < 0.01$. **d**, The percentage of PPI was assessed 3 h after the last injection of the subchronic treatment in vehicle-treated (black) and DN13-DN1-treated (red) WT and GluN1-KD mice. Data are mean \pm s.d. The number of animals is indicated above the x axis. Statistical analysis was performed using three-way rm-ANOVA followed by Tukey's HSD test compared with vehicle-treated WT mice ($n = 8$) (hash symbols) and compared with vehicle-treated GluN1-KD mice ($n = 10$) (asterisks); $^{##}P < 0.01$, $^{**}P < 0.01$, $^{***}P < 0.001$. Details of the statistical analysis and P values are provided as source data. The diagram in **a** was partly generated using Servier Medical Art, provided by Servier, under a CC 4.0 license.

at the bottom of the bar. Statistical analysis was performed using two-way MANOVA followed by Tukey's HSD test compared with vehicle-treated WT mice (hash symbols) and compared with vehicle-treated GluN1-KD mice (asterisks); $^{###}P < 0.001$, $^{**}P < 0.01$. **d**, The percentage of PPI was assessed 3 h after the last injection of the subchronic treatment in vehicle-treated (black) and DN13-DN1-treated (red) WT and GluN1-KD mice. Data are mean \pm s.d. The number of animals is indicated above the x axis. Statistical analysis was performed using three-way rm-ANOVA followed by Tukey's HSD test compared with vehicle-treated WT mice ($n = 8$) (hash symbols) and compared with vehicle-treated GluN1-KD mice ($n = 10$) (asterisks); $^{##}P < 0.01$, $^{**}P < 0.01$, $^{***}P < 0.001$. Details of the statistical analysis and P values are provided as source data. The diagram in **a** was partly generated using Servier Medical Art, provided by Servier, under a CC 4.0 license.

eliminated from circulation in less than 6 h. This reveals a fast brain entry of nanobodies and suggests that prolonging their blood stability, through fusion to an albumin-binding motif, for example³⁴, could further enhance brain penetration by lengthening the circulating half-life. In support of a better brain access of our nanobody over IgG, when combined with an Fc domain to generate an IgG-like antibody, DN13 nanobody has no effect in the animal models, further illustrating the

advantage of the small size of nanobodies. Considering the quantity of molecule administered to mice (from 1 to 20 mg per kg for DN13-DN1, 3 to 25 mg per kg for IgG) and their size difference (30 kDa and 150 kDa, respectively), a larger number of nanobody molecules is present in the brain. In the case of our Fc construct (80 kDa), the size difference is less than the difference in the dose injected (10 mg per kg, versus as low as 1 mg per kg for the nanobody) such that this difference cannot

explain per se the absence of effect of the Fc construct. The mechanism of nanobody brain penetration is not fully elucidated³⁵. It has been proposed that a basic value of nanobody isoelectric point may facilitate brain penetration. However, our preliminary study offers evidence of a passage through the fenestrated vessels, a route that cannot be used by proteins larger than 60 kDa, including IgGs (Supplementary Fig. 1). We also observed a similar brain penetration of these nanobodies in *mGlu2*^{-/-} mice, demonstrating that this target is not involved in the trafficking through the blood–brain barrier (Supplementary Fig. 2). Moreover, thanks to their small size, nanobodies have better tissue penetration than large antibodies, allowing an easier access to their target^{28,36}. The small size also confers on nanobodies access to small cavities, revealing additional epitopes compared with IgGs³⁷. Other advantages of nanobodies are their low immunogenicity^{38,39}, stability, easy expression and low-cost production⁴⁰.

Our data show that DN13–DNI can still exert in vivo effects 7 days after a single i.p. injection, consistent with the detection of the tritiated nanobody in the brain 1 week after its injection. Such a long-term effect of the nanobody is a clear advantage over the use of small-molecule agonists of mGlu2, which showed effects only acutely and no effect when tested 7 days after administration.

The mGlu2 receptor is a target that was already highly studied for the treatment of symptoms associated with schizophrenia^{17–21}. Despite the failure of the mGlu2/mGlu3 agonists²² or mGlu2 PAMs^{41,42} in phase II or phase III trials due to lack of efficacy, a post hoc analysis indicates that an epigenetic downregulation of mGlu2 receptor expression occurs after antipsychotic treatment²². It is possible that mGlu2 downregulation precluded the beneficial effect of the mGlu2/mGlu3 ligands in patients who were treated with antipsychotics, while other patients showed positive effects to mGlu2 ligands, providing new perspectives for mGlu2 targeting compounds in schizophrenia²². Our present results suggest that DN13–DNI represents an interesting alternative to small molecules. Behavioural tests indicate that the nanobody is as efficient as the mGlu2/3 agonist LY379268 for restoring cognition and sensorimotor gating in two mouse-models with schizophrenia-like symptoms resulting from NMDA receptor hypofunction. Compared with LY379268, DN13–DNI has the advantage of being selective for mGlu2 homodimers and potentiates their activation only where and when the endogenous ligand is present, thereby avoiding overstimulation and desensitization, which is often a major side effect of full agonists⁴³. Indeed, we found that acute and subchronic treatment with DN13–DNI had no effect on the mGlu2 receptor expression in various brain regions. Compared with small-molecule PAMs, the nanobody has the advantage of being hydrophilic, limiting potential off-target binding, which was reported for hydrophobic small-molecule PAMs^{44,45}. Moreover, the effect of the small-molecule PAMs on the mGlu2-containing heterodimers is largely not known and may contribute to side effects⁴⁶. Taken together, our data show that targeting mGlu2 homodimers selectively, not heterodimers or other mGlu receptors, is efficient in restoring behavioural deficits resulting from NMDA receptor hypofunction. This further supports mGlu2 homodimers as a specific target to treat patients with GRIN disorders, as well as those with schizophrenia associated with an important deficit in the glutamatergic system.

Despite the promise of nanobodies as possible therapeutic tools, more work will have to be done to minimize any possible adverse effects. The possible immunogenicity of nanobodies has already been studied and appears to be limited due to the very high conservation with human V_H class 3 (reviewed previously³⁹). However, immunogenicity has been reported for some nanobodies⁴⁷. With only 12 residues different between nanobodies and human V_H, humanization can be envisioned^{39,47}, with the limitation of residues within complementarity-determining regions. Regardless, two nanobodies are already on the market^{48,49}, including one that is fused to an anti-albumin nanobody to largely increase its residence time in the blood circulation, a situation that would favour immunogenicity. Possible peripheral effects of DN13–DNI cannot be

excluded as mGlu2 expression has been reported in some non-neuronal tissues, such as the lungs⁵⁰. However, due to the short half-life of the nanobody in the periphery, such side effects will likely be limited in time²⁸. Furthermore, it remains to be clarified which is the best format for therapeutic development of the nanobodies and which route of administration (i.v., subcutaneous or intranasal) will be preferable.

Together, our study opens new routes for the clinical management of brain diseases with nanobody-based immunotherapies using low-frequency, peripheral administration. Moreover, DN13–DNI will help us to understand cognitive deficits resulting from NMDA receptor hypofunction, such as those leading to schizophrenia or those responsible for the rare human genetic GRIN disorders, and ascertain the relevance of mGlu2 receptor activation in patient care.

Online content

Any methods, additional references, Nature Portfolio reporting summaries, source data, extended data, supplementary information, acknowledgements, peer review information; details of author contributions and competing interests; and statements of data and code availability are available at <https://doi.org/10.1038/s41586-025-09265-8>.

- Kumar, N. N. et al. Passive immunotherapies for central nervous system disorders: current delivery challenges and new approaches. *Bioconjug. Chem.* **29**, 3937–3966 (2018).
- Terstappen, G. C., Meyer, A. H., Bell, R. D. & Zhang, W. Strategies for delivering therapeutics across the blood-brain barrier. *Nat. Rev. Drug. Discov.* **20**, 362–383 (2021).
- Muyldermans, S. A guide to: generation and design of nanobodies. *FEBS J.* **288**, 2084–2102 (2021).
- Sevigny, J. et al. The antibody aducanumab reduces Aβ plaques in Alzheimer's disease. *Nature* **537**, 50–56 (2016).
- Heneka, M. T., Morgan, D. & Jessen, F. Passive anti-amyloid β immunotherapy in Alzheimer's disease—opportunities and challenges. *Lancet* **404**, 2198–2208 (2024).
- Li, T. et al. Cell-penetrating anti-GFAP VH and corresponding fluorescent fusion protein VHH-GFP spontaneously cross the blood-brain barrier and specifically recognize astrocytes: application to brain imaging. *FASEB J.* **26**, 3969–3979 (2012).
- Li, T. et al. Camelid single-domain antibodies: a versatile tool for in vivo imaging of extracellular and intracellular brain targets. *J. Control. Release* **243**, 1–10 (2016).
- Muruganandam, A., Tanha, J., Narang, S. & Stanimirovic, D. Selection of phage-displayed llama single-domain antibodies that transmigrate across human blood-brain barrier endothelium. *FASEB J.* **16**, 240–242 (2002).
- Caljon, G. et al. Using microdialysis to analyse the passage of monovalent nanobodies through the blood-brain barrier. *Br. J. Pharmacol.* **165**, 2341–2353 (2012).
- Tsitokana, M. E., Lafon, P.-A., Prézeau, L., Pin, J.-P. & Rondard, P. Targeting the brain with single-domain antibodies: greater potential than stated so far? *Int. J. Mol. Sci.* **24**, 2632 (2023).
- Scholler, P. et al. Allosteric nanobodies uncover a role of hippocampal mGlu2 receptor homodimers in contextual fear consolidation. *Nat. Commun.* **8**, 1967 (2017).
- Haubrich, J. et al. A nanobody activating metabotropic glutamate receptor 4 discriminates between homo- and heterodimers. *Proc. Natl. Acad. Sci. USA* **118**, e2105848118 (2021).
- McMahon, C. et al. Synthetic nanobodies as angiotensin receptor blockers. *Proc. Natl. Acad. Sci. USA* **117**, 20284–20291 (2020).
- Jähnichen, S. et al. CXCR4 nanobodies (VHH-based single variable domains) potently inhibit chemotaxis and HIV-1 replication and mobilize stem cells. *Proc. Natl. Acad. Sci. USA* **107**, 20565–20570 (2010).
- Ma, Y. et al. Structure-guided discovery of a single-domain antibody agonist against human apelin receptor. *Sci. Adv.* **6**, eaax7379 (2020).
- Reiner, A. & Levitz, J. Glutamatergic signaling in the central nervous system: ionotropic and metabotropic receptors in concert. *Neuron* **98**, 1080–1098 (2018).
- Ellaithy, A., Younkin, J., González-Maeso, J. & Logothetis, D. E. Positive allosteric modulators of metabotropic glutamate 2 receptors in schizophrenia treatment. *Trends Neurosci.* **38**, 506–516 (2015).
- Dogra, S. & Conn, P. J. Metabotropic glutamate receptors as emerging targets for the treatment of schizophrenia. *Mol. Pharmacol.* **101**, 275–285 (2022).
- Patil, S. T. et al. Activation of mGlu2/3 receptors as a new approach to treat schizophrenia: a randomized phase 2 clinical trial. *Nat. Med.* **13**, 1102–1107 (2007).
- Adams, D. H. et al. A long-term, phase 2, multicenter, randomized, open-label, comparative safety study of pomaglumetad methionil (LY2140023 monohydrate) versus atypical antipsychotic standard of care in patients with schizophrenia. *BMC Psychiatry* **13**, 143 (2013).
- Kinon, B. J. et al. A multicenter, inpatient, phase 2, double-blind, placebo-controlled dose-ranging study of LY2140023 monohydrate in patients with DSM-IV schizophrenia. *J. Clin. Psychopharmacol.* **31**, 349–355 (2011).
- Kinon, B. J., Millen, B. A., Zhang, L. & McKinzie, D. L. Exploratory analysis for a targeted patient population responsive to the metabotropic glutamate 2/3 receptor agonist pomaglumetad methionil in schizophrenia. *Biol. Psychiatry* **78**, 754–762 (2015).
- Lin, S. et al. Structures of Gi-bound metabotropic glutamate receptors mGlu2 and mGlu4. *Nature* **594**, 583–588 (2021).

24. Nakatani-Pawlak, A., Yamaguchi, K., Tatsumi, Y., Mizoguchi, H. & Yoneda, Y. Neonatal phencyclidine treatment in mice induces behavioral, histological and neurochemical abnormalities in adulthood. *Biol. Pharm. Bull.* **32**, 1576–1583 (2009).
25. Ramsey, A. J. NR1 knockdown mice as a representative model of the glutamate hypothesis of schizophrenia. *Prog. Brain Res.* **179**, 51–58 (2009).
26. Mohn, A. R., Gainetdinov, R. R., Caron, M. G. & Koller, B. H. Mice with reduced NMDA receptor expression display behaviors related to schizophrenia. *Cell* **98**, 427–436 (1999).
27. Wright, R. A. et al. CNS distribution of metabotropic glutamate 2 and 3 receptors: transgenic mice and [³H]LY459477 autoradiography. *Neuropharmacology* **66**, 89–98 (2013).
28. Jovčevska, I. & Muyldermans, S. The therapeutic potential of nanobodies. *BioDrugs* **34**, 11–26 (2020).
29. Bickel, S., Lipp, H.-P. & Umbricht, D. Early auditory sensory processing deficits in mouse mutants with reduced NMDA receptor function. *Neuropsychopharmacology* **33**, 1680–1689 (2008).
30. Duncan, G. E. et al. Deficits in sensorimotor gating and tests of social behavior in a genetic model of reduced NMDA receptor function. *Behav. Brain Res.* **153**, 507–519 (2004).
31. Fradley, R. L. et al. STOP knockout and NMDA NR1 hypomorphic mice exhibit deficits in sensorimotor gating. *Behav. Brain Res.* **163**, 257–264 (2005).
32. Ilanges, A. et al. Brainstem ADCYAP1^r neurons control multiple aspects of sickness behaviour. *Nature* **609**, 761–771 (2022).
33. Wei, C. et al. Brain endothelial GSDMD activation mediates inflammatory BBB breakdown. *Nature* **629**, 893–900 (2024).
34. Tijink, B. M. et al. Improved tumor targeting of anti-epidermal growth factor receptor Nanobodies through albumin binding: taking advantage of modular Nanobody technology. *Mol. Cancer Ther.* **7**, 2288–2297 (2008).
35. Pothin, E., Lesuisse, D. & Lafaye, P. Brain delivery of single-domain antibodies: a focus on VH and VNAR. *Pharmaceutics* **12**, 937 (2020).
36. Debie, P. et al. Size and affinity kinetics of nanobodies influence targeting and penetration of solid tumours. *J. Control. Release* **317**, 34–42 (2020).
37. Uchański, T., Pardon, E. & Steyaert, J. Nanobodies to study protein conformational states. *Curr. Opin. Struct. Biol.* **60**, 117–123 (2020).
38. Cortez-Retamozo, V. et al. Efficient tumor targeting by single-domain antibody fragments of camels. *Int. J. Cancer* **98**, 456–462 (2002).
39. Ackaert, C. et al. Immunogenicity risk profile of nanobodies. *Front. Immunol.* **12**, 632687 (2021).
40. Pardon, E. et al. A general protocol for the generation of nanobodies for structural biology. *Nat. Protoc.* **9**, 674–693 (2014).
41. Litman, R. E. et al. AZD8529, a positive allosteric modulator at the mGluR2 receptor, does not improve symptoms in schizophrenia: a proof of principle study. *Schizophr. Res.* **172**, 152–157 (2016).
42. Salih, H. et al. Pharmacokinetic and pharmacodynamic characterisation of JNJ-40411813, a positive allosteric modulator of mGluR2, in two randomised, double-blind phase-I studies. *J. Psychopharmacol.* **29**, 414–425 (2015).
43. Christopoulos, A. Advances in G protein-coupled receptor allostericity: from function to structure. *Mol. Pharmacol.* **86**, 463–478 (2014).
44. Belhocine, A. et al. Profiling of orthosteric and allosteric group-III metabotropic glutamate receptor ligands on various G protein-coupled receptors with Tag-lite® assays. *Neuropharmacology* **140**, 233–245 (2018).
45. Hellyer, S. D. et al. Selective' class C G protein-coupled receptor modulators are neutral or biased mGlu5 allosteric ligands. *Mol. Pharmacol.* **93**, 504–514 (2018).
46. Yin, S. et al. Selective actions of novel allosteric modulators reveal functional heteromers of metabotropic glutamate receptors in the CNS. *J. Neurosci.* **34**, 79–94 (2014).
47. Rossotti, M. A., Bélanger, K., Henry, K. A. & Tanha, J. Immunogenicity and humanization of single-domain antibodies. *FEBS J.* **289**, 4304–4327 (2022).
48. Duggan, S. Caplacizumab: first global approval. *Drugs* **78**, 1639–1642 (2018).
49. Tsumoto, K. & Takeuchi, T. Next-generation anti-TNF α agents: the example of ozoraliizumab. *BioDrugs* **38**, 341–351 (2024).
50. Wang, J. et al. SARS-CoV-2 uses metabotropic glutamate receptor subtype 2 as an internalization factor to infect cells. *Cell Discov.* **7**, 119 (2021).

Publisher's note Springer Nature remains neutral with regard to jurisdictional claims in published maps and institutional affiliations.



Open Access This article is licensed under a Creative Commons Attribution-NonCommercial-NoDerivatives 4.0 International License, which permits any non-commercial use, sharing, distribution and reproduction in any medium or format, as long as you give appropriate credit to the original author(s) and the source, provide a link to the Creative Commons licence, and indicate if you modified the licensed material. You do not have permission under this licence to share adapted material derived from this article or parts of it. The images or other third party material in this article are included in the article's Creative Commons licence, unless indicated otherwise in a credit line to the material. If material is not included in the article's Creative Commons licence and your intended use is not permitted by statutory regulation or exceeds the permitted use, you will need to obtain permission directly from the copyright holder. To view a copy of this licence, visit <http://creativecommons.org/licenses/by-nc-nd/4.0/>.

© The Author(s) 2025

Article

Methods

Ethics

Animal care and surgical procedures were performed according to the Directive 2010/63/EU of the European Parliament, which had been approved by the Ministry of Agriculture, France. The project was approved by the French National Ethics Committee for Animal Experimentation (CEEA) under the number APAFIS 36241-2022032518526906 v4 (for PCP procedure), APAFIS 4111-2016021613253432 v5 (for tritiated nanobodies) and APAFIS 31981-2021060423426200 v3 (for nanobody pharmacokinetics in blood). Behavioural pharmacology in GluN1-KD mice was approved by the Faculty of Medicine and Pharmacy Animal Care Committee at the University of Toronto in accordance with Canadian Council on Animal Care (CCAC) guidelines. All experiments were performed in accordance with relevant named guidelines and regulations.

Animals

C57BL/6J WT mice (21.5 ± 0.3 g) were purchased from Janvier Labs. GluN1-KD mice (*Grin1* KD) were generated as previously described²⁶. Congenic C57BL/6J *Grin1*^{+/+} and 129 × 1/SvJ *Grin1*^{+/+} mice were intercrossed to produce experimental mice (*Grin1*^{+/+} (WT) and Grin1-KD) mice as recommended and based on other studies^{51,52} to minimize the confound of homozygous mutations on each parental strain. Animals were housed under a 12 h–12 h light–dark cycle, at 22 ± 1 °C and $55 \pm 10\%$ of relative humidity. All animals had access to water and food ad libitum.

Reagents, cell lines, antibodies and plasmids

HEK293 cells (ATCC, CRL-1573) were cultivated in DMEM or DMEM-GlutaMAX (Life Technologies) complemented with 10% (v/v) fetal bovine serum (Sigma-Aldrich). Absence of mycoplasma was routinely checked using MycoAlert Mycoplasma detection kit (LT07-318, Lonza) according to the manufacturer's protocol. The pRK5 plasmid encoding WT rat mGlu2 receptor subunit, with an HA-tag and a SNAP inserted just after the signal peptide, was previously described⁵³. All drugs (LY379268 and LY341495) were from Tocris (Bio-technne). HTRF IP-One Gq Detection Kit (62IPAPEB), HTRF anti-6×His monoclonal antibody d2-conjugate (61HISDLA), Tag-lite SNAP-Lumi4-Tb Labelling Reagent (SSNPTBD), HTRF d2-NHS (65D2SABA) were gifted by Revvity. Monoclonal rabbit anti-6×His, 3,3'-diaminobenzidine chromogen solution (DAB) peroxidase substrate kit and ABC peroxidase kit (anti-rabbit-HRP) were purchased from Invitrogen and Vector Laboratories, respectively.

Plasmid of nanobodies constructs

Bivalent nanobodies were obtained by fusing one copy of DN1, DN10 or DN13 to either the N or C terminus of DN13 using one of the two linkers. A 6×His-tag was inserted at the C terminus of the second nanobody for purification purposes. The sequences of the linkers are as follows: hinge HcAb (EPKIPQPQPKPQPQPKPQPKPEP) or (GGGGS)₃: GGGGSGGGSGGGGS. The bivalent DN13–DN13 constructs with the two different linkers were synthesized by Genecust and cloned between NdeI and Xhol in a modified pHEN1 vector in which the sequence coding for the G3P protein has been removed. The bivalent biparatopic constructs were generated by PCR and subcloned through silent restriction sites inserted into the framework regions FR1 and FR4. To generate the cDNA of DN13–Fc, the monomeric DN13 sequence was inserted into the pcDNA3.1(+) vector with the secretory signal peptide from human interleukin (IL-2) fused to its N terminus and the sequence encoding the Fc region of human IgG1 at its C terminus.

Production and purification

For large scale nanobody production, plasmids encoding nanobodies were transformed in *E. coli* BL21DE3 strain (Life technologies). A single colony was grown in 10 ml of LB, supplemented with 100 µg ml⁻¹ ampicillin, 1% (w/v) glucose, overnight at 37 °C with shaking. Then 1 l of LB

supplemented with around 10 ml of the preculture was incubated until an optical density at 600 nm (OD₆₀₀) of 0.6–0.7. The nanobody expression was induced with 1 mM isopropyl β-D-1-thiogalactopyranoside and bacteria were grown overnight at 28 °C with shaking. Bacteria were collected by centrifugation for 10 min at 5,000g, resuspended in 10 ml per 1 l culture of ice-cold TES buffer (0.2 M Tris, 0.5 mM EDTA, 0.5 M sucrose, pH 8) and incubated for at least 1 h at 4 °C on shaking platform. Then, 20 ml per 1 l of culture of TES/4 (TES buffer diluted four times in water) were added to the solution and further incubated for at least 45 min at 4 °C on a shaking platform. The periplasmic extract was recovered by collecting the supernatant after centrifugation of the suspension for 30 min at 10,000g at 4 °C.

To produce DN13–Fc, HEK293F cells (Expi293 Expression System Kit, A14635, Thermo Fisher Scientific) were cultured at a density of 0.6×10^6 cells per ml with 180 ml fresh medium in a 2 l culture bottle at 37 °C and 5% CO₂, shaken at 200 rpm, as previously described for DN42–Fc⁵⁴. Of the cells, $1-1.5 \times 10^6$ cells per ml were transfected with DN13–Fc plasmid (225 µg in 12 ml OMEM) and PEI (675 µg in 733 ml OMEM). Cells were cultured for 4–7 days at 37 °C and 5% CO₂ with 200 rpm shaking. The supernatant was collected after a 10 min centrifugation at 2,000g and 4 °C.

The His-tagged nanobodies from bacteria and HEK293F cells were purified from the periplasmic extract or cell supernatants using Ni-NTA purification (Qiagen) according to the manufacturer's instructions. Desalting was performed using disposable PD-10 desalting columns (Cytiva) according to the manufacturer's instructions to obtain the nanobodies in phosphate buffer solution. Endotoxins were removed using Proteus NoEndo S (Generon) according to the manufacturer's instructions before administration of the nanobodies to animals. Part of DN13–DN1 produced followed a second step of purification by size-exclusion chromatography using gel filtration (ÄKTA, Cytiva) before administration of the nanobodies to animals to reduce further endotoxin content.

LPS quantification

E. coli LPS contamination was assessed by targeted quantification of 3-hydroxy myristic acid (3-OHC14:0) as previously described⁵⁵ with modifications⁵⁶. In brief, protein aliquots (100 µl, 200–500 µg) were spiked with 20 pmol of 3-hydroxytridecanoic acid (3OH-C13:0, 1 pmol µl⁻¹ in ethanol) used as an internal standard (IS). The samples were then hydrolysed with 8 M hydrochloric acid (300 µl) for 3 h at 90 °C. Released fatty acids were extracted with 600 µl of endotoxin-free water and ethyl acetate:hexane 3:2 (v/v; 5 ml). The organic phases were dried in vacuo. Dried extracts were finally solubilized in 50 µl ethanol and 3 µl were injected into a liquid chromatography–tandem mass spectrometry system as described previously⁵⁶. Calibration standards (100 µl PBS) containing 0, 0.5, 1, 2, 4, 8, 16, 32 and 64 pmol 3OH-C14:0 were treated as samples. The area under the curves for 3OHC14:0 and 3OH-C13:0 (IS) was determined, and the area ratios 3OH-C14:0/IS were calculated. A linear calibration was used for the calculations. LPS concentration was calculated assuming a molecular mass of 12,000 g mol⁻¹ and that each LPS molecule contains four molecules of 3OH-C14:0. One endotoxin unit (EU) is considered to be equivalent to 0.1 ng of LPS.

Binding experiments based on TR-FRET

HEK293 cells were transfected with cDNA encoding rat, human or mouse SNAP-tagged mGlu2 receptors and the high-affinity glutamate transporter EAAC1. Then, 24 h after transfection, cells were labelled in 150 mm cell culture plates with 100 nM Tag-lite SNAP-Lumi4-Tb Labelling Reagent in DMEM-GlutaMAX for 1 h at 37 °C, and washed three times with Krebs buffer (10 mM HEPES pH 7.4, 146 mM NaCl, 4.2 mM KCl, 1 mM CaCl₂, 0.5 mM MgCl₂, 5.6 mM glucose and 0.1% BSA). Cells were detached using cell-dissociation buffer (Sigma-Aldrich) transferred at 10,000 cells per well in a white 384-well plate (Greiner bio-one, PS,

F-bottom, small volume). Increasing concentrations of 6×His-tagged nanobodies, together with either 1 μM LY379268 (agonist) or 1 μM LY341495 (antagonist) and with 200 nM of HTRF anti-6×His monoclonal antibody d2-conjugate, were applied to Lumi4-Tb-labelled cells in a final volume of 20 μl overnight at 20 °C.

To determine the selectivity of the DN13–DN1 nanobody for the mGlu1–8 receptors, HEK293 cells were transfected with cDNA encoding for human SNAP-tagged mGlu receptors and transferred at 10⁵ cells per well in a black 96-well plate (Greiner bio-one, PS, F-bottom), as previously described³⁴. Then, 24 h after transfection, cells were labelled with 100 nM Tag-lite SNAP-Lumi4-Tb Labelling Reagent in DMEM-GlutaMAX for 1 h at 37 °C, and washed three times with Krebs buffer. Next, 200 nM of 6×His-tagged DN13–DN1 and 300 nM of anti-6×His-d2, and the agonists (1 μM quisqualic acid for mGlu1 and mGlu5; 1 μM LY379268 for mGlu2 and mGlu3; 100 μM L-AP4 for mGlu4, mGlu6, mGlu7 and mGlu8) or the antagonist (10 μM LY341495) were added to the cells in a total volume of 60 μl per well, and incubated overnight at 20 °C.

FRET signals were determined by measuring the sensitized acceptor emission (665 nm) and Tb donor emission (620 nm) using a 50 μs delay and 450 μs integration time after excitation at 337 nm on a PHERAstar FS plate-reader (BMG LabTech) using PHERAstar control software v.5.41. TR-FRET ratio (665 nm/620 nm × 10⁴, patent Cisbio Bioassays, US5,527,684) was calculated for preventing interferences due to medium variability and chemical compound or to normalize experiments when using cells expressing different receptor levels.

Measurements of inositol phosphate

HEK293 cells were co-transfected by electroporation with plasmids encoding rat, human or mouse SNAP-tagged mGlu2 receptors, EAAC1 and GqTop to allow efficient coupling of mGlu2 to the phospholipase C pathway. In total, 100,000 cells were used per well in a black 96-well plate (Greiner bio-one, PS, F-bottom). Then, 24 h after transfection at 37 °C, cells were washed and stimulated with EC₂₀ LY379268 (for human, 0.48 nM; mouse, 0.63 nM; rat, 0.6 nM) or EC₂₀ glutamate (for human, 3.58 μM; mouse, 10.18 μM; rat, 5.42 μM) and various concentrations of nanobodies and incubated for 30 min at 37 °C and 5% CO₂. The measurement of IP1 accumulation was determined using the HTRF IP-One Gq Detection Kit (Revvity) according to the manufacturer's recommendations.

Fluorescent nanobody labelling

Nanobodies were dialysed overnight at 4 °C in carbonate buffer (0.1 mM, pH 9) and incubated (250 μg nanobodies at 2 mg ml⁻¹) with the fluorophore HTRF d2-NHS (Revvity) in phosphate buffer (100 mM pH 7) at a ratio of 6 (fluorophore/nanobody), for 45 min at 25 °C; or in phosphate buffer (50 mM pH 8) and incubated with Lumi4-Tb-NHS (Revvity) in phosphate buffer (100 mM pH 7) at a ratio of 12 for 30 min at 25 °C. Nanobodies were purified by gel filtration column (NAP-5, GE Healthcare) in phosphate buffer 100 mM pH 7. The final molar ratio of fluorophores per nanobody was calculated as the fluorophore concentration/conjugated nanobody concentration, and the conditions were set up for a ratio of between 2 and 3. The concentration of fluorophores in the labelled fraction was calculated for each fluorophore as the OD/ε (OD₆₅₀ and ε = 225,000 M⁻¹cm⁻¹ for d2, and OD₃₄₀ and ε = 26,000 M⁻¹cm⁻¹ for Lumi4-Tb), while that of nanobodies was determined by the OD₂₈₀. The conjugated concentration was calculated as OD₂₈₀ – (OD_{fluor}/R_{zmax})/ε nanobody with R_{zmax} = OD_{fluor}/OD₂₈₀. The average number of fluorophores is 2.5 per DN13–DN1. The purified labelled fraction was supplemented with 0.1% BSA and kept at –20 °C.

Histological processing of brains

WT C57BL/6J mice were purchased from Janvier Labs. Brains from *mGlu2*^{−/−} mice were provided by J. Gonzalez-Maeso (Virginia Commonwealth University). Mice were anaesthetized (Euthasol Vet 8%, Alcyon) and euthanized by a cardiac perfusion of 4% paraformaldehyde (PFA).

Brains were extracted and fixed in a 4% PFA solution (Euromedex) overnight at 4 °C. The brains were rinsed in PBS and cryoprotected in a 30% sucrose solution for 4 days at 4 °C. The brains were then added to OCT (Tissue-Tek, Sakura Finetek), quickly frozen in acetone chilled on dry ice and conserved at –80 °C until use. The frozen brains in OCT were moved to –20 °C 24 h before cryo-sectioning. They were mounted onto a cryostat (Leica) and 16 μm sagittal sections were performed and directly mounted on Superfrost Plus glass slides (Sigma-Aldrich) and kept at –20 °C until use. For immunofluorescence experiments, sagittal brain tissue sections of WT and *mGlu2*^{−/−} mice were blocked 1 h at 25 °C with a blocking solution (3% BSA, 0.1% Triton X-100 in PBS) and incubated with DN13–DN1–d2 (200 nM), overnight at 4 °C, to label mGlu2 receptors. The sections were washed with PBS, then with distilled water and mounted using Fluoroshield containing DAPI to stain nuclei (Sigma-Aldrich). Images were taken using a slide scanner Axio scan Z1 microscope (Zeiss, Jena) by performing full-section mosaics with a 20× enlargement with Zeiss Zen software 2.3 light. For immunohistochemistry experiments, C57BL/6J female WT mice were injected i.p. either with 10 mg per kg of DN13–DN1 or with an equivalent volume of PBS (150 μl) as a negative control. Then, 24 h after injection, mice were anaesthetized (Euthasol Vet 8%) and euthanized as described above. Ten glass slides per animal, each containing five brain tissue sections, with 80 μm spacing between each section, were rinsed with Tris-buffered saline (TBS) and incubated 1 h at 25 °C with a blocking solution (5% normal goat serum, 0.1% Triton X-100 in TBS). The sections were then incubated with a monoclonal rabbit anti-6×His (1:500, Life Technologies) 2 h at 25 °C and washed in TBS. After blocking endogenous peroxidase (3% H₂O₂ solution, 20 min at 25 °C), the sections were incubated with a goat anti-rabbit biotinylated antibody (1:100, ABC peroxidase kit, Vector Laboratories). Labelling was revealed using the DAB peroxidase substrate kit (Vector Laboratories). The sections were then washed in distilled water and mounted using Fluoroshield with DAPI. Images were taken using a slide scanner Axio scan Z1 microscope by performing full-section mosaics with ×20 enlargement.

Nanobody quantification in the blood

A quantitative test assessing nanobody concentration has been developed based on the TR-FRET-binding assay on cells expressing SNAP-tagged mGlu2 receptor. To determine the linearity of the assay, increasing concentrations of DN13 or DN13–DN1 were added to 10,000 cells expressing Lumi4-Tb-labelled SNAP-tagged mGlu2, 200 nM of anti-6×His-d2 antibody and 1 μM LY379268 in a 384-well plate. After 3 h incubation at 20 °C, the HTRF signal was recorded on a Pherastar FS plate reader and the linearity determined using GraphPad Prism. C57BL/6J WT mice (Janvier Labs) were treated by i.p. administration of 10 mg per kg of DN13, DN13–DN1 or an equivalent volume of PBS (150 μl) and blood samples were collected at different timepoints (1 h, 2 h, 4 h, 6 h, 8 h, 10 h, 12 h and 24 h). The plasma was extracted using a microvette CB 300 K2E (Sarstedt) and frozen until use. Plasma (3 μl) was applied to cells expressing mGlu2 receptor, labelled with Tag-lite SNAP-Lumi4-Tb Labelling Reagent in the presence of 200 nM of HTRF anti-6×His monoclonal antibody d2 conjugate. The FRET signal was determined as indicated for the saturation binding assay.

Nanobody radiolabelling

DN13–DN1 was radiolabelled using bacterial transglutaminase and a synthetic peptide tag, CBz-Gln-Gly-Lys-OH synthetized using manual solid-phase peptide synthesis on a microwave synthesizer (CEM) according to a standard Fmoc-based synthesis protocol. Starting from the Fmoc-Lys(Boc)-Wang resin loaded at 0.32 mmol g⁻¹ (Novabiochem), the synthesis was performed on a 0.015 mmol per reactor scale. Protected amino acids Fmoc-Gly-OH and CBz-Gln-OH (5 eq.) were coupled using HATU (4.5 eq.) and iPr₂EtN (10 eq.) in DMF for 20 min at 60 °C. The Fmoc group was deprotected by three successive treatments with

Article

20% piperidine in DMF for 3 min. The peptide was then deprotected and cleaved from the resin by a treatment with trifluoroacetic acid/H₂O/triisopropylsilane (95/2.5/2.5) for 2 h at 25 °C. The peptide was then precipitated by dilution into an ice-cold diethyl ether solution, recovered by centrifugation and washed twice with diethyl ether. CBz-Gln-Gly-Lys-OH was tritiated using the following procedure. To a solution of the CBz-protected peptide (87 nmol, 1 eq.) in DMF (50 µl) at 25 °C was added iPr₂EtN (870 nmol, 10 eq.) and [³H]N-(propionyloxy)succinimide (87 nmol, 1 eq.). The mixture was stirred at 25 °C for 2 h. The labelled product was purified on a high-performance liquid chromatography system equipped with a Luna Omega C18 (150 × 4.6 mm; 3 µm) column (Phenomenex) with a gradient of 0–100% buffer B in buffer A over 20 min with a flow rate of 1 ml min⁻¹ (buffer A: 0.1% formic acid in H₂O; buffer B: 0.1% formic acid in acetonitrile). The radiolabelling of DN13–DN1 through lysine conjugation was carried out in PBS buffer at pH 7.4 using 1 U per 20 nmol of bacterial transglutaminase (Zedira), 2 eq. of the radiolabelled peptide tag and 80 µM of DN13–DN1. The mixture was then incubated for 2 h at 25 °C. After incubation, the labelled protein was purified on Protino Ni-NTA resin (Macherey-Nagel) and then the buffer was exchanged to 0.9% (w/v) NaCl using an Amicon centrifugal filter (Merck) for in vivo experiments. Part of the labelled DN13–DN1 was digested by trypsin to identify Lys121 of the ERK motif in the hinge HcAb, as the conjugation site by MALDI-TOF (Thermo Fisher Scientific) analysis.

In vivo cerebral quantification and localization of the tritiated nanobody and autoradiography

Experiments were conducted on adult female WT C57BL/6J mice (18.8 ± 0.2 g) purchased from Janvier Labs. Mice were injected i.p. with 10 mg per kg of [³H]DN13–DN1 (3 µCi) or vehicle in 50 µl. The mice were euthanized 4 h, 24 h, 4 days or 7 days after administration (only at 24 h for vehicle group), perfused with 0.9% (w/v) NaCl (10 ml per mouse, 200 ml h⁻¹) for brain collection and freezing. Brains were used for either tissue quantification or cerebral localization of β-radioactivity. Quantification of β-radioactivity contained in total brain homogenate was performed using a liquid scintillation analyzer (Tri-Carb 2100TR, Packard BioScience) using QuantaSmart (v.5.2). Brain tissue sections (thickness, 20 µm) were prepared on a slicing microtome (Leica Microsystems) to perform imaging and observe cerebral localization by digital autoradiography with a high-performance β-Imager (Biospace Lab) using Beta-Acquisition software (v.9.4.12.219) allowing real-time [³H] radioactive imaging through direct β-particle counting in dried tissue sections (detection threshold of 0.007 cpm mm⁻²).

NOR test on a neurodevelopmental mouse model of schizophrenia induced by PCP administration

Male and female mice used were C57BL/6J mice (Janvier Labs) and were injected subcutaneously with 10 mg per kg of phencyclidine (PCP mice) (Sigma-Aldrich, ANSM authorization, A-2018-3-330-S) or with a saline solution (0.9% (w/v) NaCl) (control mice) at postnatal day 7 (P7), P9 and P11. At adulthood, 1 week before the test, the mice were extensively handled by the operator: the first 2 days, the operator put his hand on the home cage of the animals to familiarize the animals to his presence and, the following days, the animals were handled few minutes per day. NOR testing was carried out in an open field, consisting of four compartments of 50 × 50 cm, each containing one mouse, placed in a dimly lit room with clearly visible contextual cues (black on white patterns) on the surrounding walls. Each mouse was habituated to the arena for 10 min the day before the training session. Mice then performed the NOR task. After a 5-min training session, a 24-h or a 7-day retention interval was observed, during which the mice were transferred back to the home cage and the arena and objects were cleaned. During the test session, the animals were placed back into the arena in the presence of an identical copy of one of the familiar objects and a novel object and allowed to explore the objects freely for 5 min. The objects were

plastic toys (approximately 3 cm width, 3 cm length, 5 cm height) and were cleaned with 10% ethanol between sessions. The experiments were video-recorded (EthoVision XT 13.0, Noldus; Logitech Capture v.2.08.11) and exploration times (nose in contact or sniffing at <1 cm) were measured by a blinded observer using a virtual timer (XNote Timer v.1.12.0.0). Mice with a total time exploration of less than 3 s in the test session were excluded. Discrimination indexes ((exploration time of novel object – exploration time of familiar object)/total object exploration time) were compared between groups. For acute treatment, i.p. administration of LY379268 (1 mg per kg) was done 1 h before the training and testing session; i.p. administration of DN13–DN1 (10 mg per kg) was done once 3 h before the training session with the objects; and LY341495 (3 mg per kg) was applied 30 min before DN13–DN1 administration. The second test was performed after a 7-day interval without further compound administration. i.c.v. administration of DN13–DN1 or DN1 (4 pmol in 5 µl) was done 24 h before the training session through a cannula that was implanted 7 days earlier. Cannula implantation was performed on mice anaesthetized with a mixture of ketamine (Imalgene 500, 50 mg ml⁻¹, Merial) and xylazine (Rompun 2%, 20 mg ml⁻¹, Bayer) diluted in 0.9% (w/v) NaCl solution (saline) (2:2:1, i.p., 0.1 ml per 30 g) and mounted onto a stereotaxic apparatus using flat skull coordinates⁵⁷. Stainless steel guide cannula (22 gauge, 5.00 mm, World Precision Instruments) were implanted in the ventricle (anteroposterior = -0.5 mm; mediolateral = 1.1 mm; dorsoventral = -2.2 mm). Cannulas were implanted vertically in the coronal plane to avoid damage to the wall of the lateral ventricle. The guide cannula was fixed to the skull with anchor screws and dental acrylic (AgnTho's). Mice could recover for a minimum of 7 days before behavioural testing. Subchronic drug administration consisted of an initial i.p. administration of DN13–DN1 (10 mg per kg) followed by three injections at 1 mg per kg, each injection spaced 1 week apart. The last injection was performed 24 h before the training session and 48 h before the testing session with the objects.

Y-maze test on the genetic mouse model GluN1-KD mice

GluN1-KD mice and their WT littermates' mice were injected i.p. with LY379268 (1 mg per kg) or DN13–DN1 (20 or 10 mg per kg) 1 h and 3 h before the test, respectively (cohort 1). Independent cohorts of mice were treated with these compounds (LY379268 and DN13–DN1) 7 days before the behavioural test (cohort 2). Subchronic drug administration consisted of an initial i.p. administration of DN13–DN1 (10 mg per kg) followed by three injections at 1 mg per kg, each injection spaced 1 week apart. The last injection was performed 3 h before the behavioural test. Working memory was assessed in a Y-maze as described previously⁵⁸. The Y-maze consisted of three equivalent arms (38 × 7.6 × 12.7 cm; San Diego Instruments) that were symmetrically disposed at 120° angles from each other. The maze floor and walls were constructed from opaque-white Plexiglas and posters with distinctive geometric shapes (6 × 9 cm) were placed at the end of each arm of the Y-maze. A mouse was initially placed into one arm and the sequence (such as ABCCAB) and the number of arm entries were recorded for 5 min. Results were collected semiautomatically using video-tracking software (Biobserve Viewer v.2.0). Arm entries were defined as all four paws entering the arm. Spontaneous alternation refers to visiting all three arms in sequence (that is, ABC or CAB but not CBC). The percentage of alternations was defined according to the following equation: percentage alternation = [(number of alternations)/(total arm entries - 2)] × 100. The number of arm entries serves as an indicator of ambulation.

PPI of the acoustic startle response test on the genetic mouse model GluN1-KD mice

The test was performed twice on the same cohort of GluN1-KD mice (cohort 3): the first test was performed on the days of LY379268 and DN13–DN1 administration and the second test was performed after a

7-day interval without further compound administration. LY379268 (1 mg per kg) and DN13-DN1 (20 or 10 mg per kg) were administered i.p. only once 1 h and 3 h before the first test, respectively. Subchronic drug administration consisted of an initial i.p. administration of DN13-DN1 (10 mg per kg) followed by three injections at 1 mg per kg, with each injection spaced 1 week apart. The last injection was performed 3 h before the behavioural test. The PPI was measured in four sound-attenuated chambers (SR-LAB ABS System, San Diego Instruments) as described previously^{58,59} and using SR_LAB Analysis software (San Diego Instruments, 6300-0000-Y). Pulse-only trials consisted of a single white noise burst (120 dB, 40 ms). Prepulse + pulse trials (PP69P, PP72P and PP81P) consisted of a prepulse of white noise (20 ms at 69 dB, 72 dB and 81 dB respectively) that was followed 100 ms after prepulse onset by a startling pulse (120 dB, 40 ms). No-stimulus trials consisted of background noise only (65 dB). The sessions were structured as follows: (1) 5-min acclimatization at background noise level; (2) five pulse trials; (3) ten blocks each containing all eight trials (Pulse, PP69; PP69P, PP72, PP72P, PP81; PP81P, No-Pulse) in pseudorandom order; and (4) five pulse trials. The force intensity for each trial was recorded as the startling level. The percentage of PPI induced by each pre-pulse intensity was calculated as $[1 - (\text{startle amplitude on prepulse trial}) / (\text{startle amplitude on pulse alone})] \times 100\%$. The same cohort of mice was tested in PPI after 3 h and retested 7 days later as post-drug-treatment intervals, as PPI is not affected by retesting⁶⁰.

Locomotor activity

For the neurodevelopmental mouse model of schizophrenia, horizontal activity was measured for 60 min in a non-stressful environmental, in a circular corridor (Imetronic). Counts for horizontal activity were incremented by consecutive interruption of two adjacent beams (mice moving through one-quarter of the circular corridor). Locomotor activity was assessed at 3 h after injection of the different nanobodies. For the genetic mouse model GluNI-KD mice, an open-field test was used to assess the locomotor activity as previously described⁶¹ under dim light (30 Lux). Test mice were placed into a novel environment—clear Plexiglas chambers measuring 20 × 20 × 45 cm—for 1 h. Their locomotor activity was recorded and tracked by digital activity monitors from Omnitech Electronics through infrared beam sensors. The distance travelled was analysed in 5 min bins to assess locomotor activity. Locomotor activity was assessed 3 h after injection of the different nanobodies.

Inclined platform

A mouse was placed onto a wire platform (1 cm × 1 cm mesh), which was then inclined to 45°. The time it took for a mouse to traverse the entire 24 cm length of the platform was recorded. Mice that fell off the inclined platform were assigned a time of 120 s (ref. 62).

Rotarod

Mice were placed onto an accelerating rotarod (Ugo Basile) and were observed at an initial speed of 4 rpm for 30 s. The rod was then gradually accelerated at a rate of 0.2 rpm s⁻¹. The latency to fall was recorded with a cut-off time of 3 min. Mice were given 3 trials with 10 min rests between trials. The latency to fall for each mouse was counted by averaging over the three trials⁶².

Pinch-induced catalepsy

Pinch-induced catalepsy was induced as originally described⁶³. A mouse was firmly pinched by the scruff of the neck with a thumb and a forefinger for 5 s. The mouse then was gently placed onto parallel wooden bars (diameter 0.5 cm), with its front paws positioned at 45° angle above the hind paws and elevated for 8 cm above the experimental table. The duration of freezing (catalepsy) was recorded for up to 2 min per trial. Each animal was tested in 3 trials with 2 min intervals. The average duration of catalepsy was analysed.

Brain tissue preparation and cell dissociation

After acute or subchronic treatment, mice were euthanized by cervical dislocation, and the brains were collected and dissected in cold PBS (pH 7.4) as previously described⁵⁴. For each brain, different regions were dissected: olfactory bulbs, prefrontal cortex, cortex, striatum, hippocampus, cerebellum and midbrain. Samples were collected in a 1.5 ml cryogenic tube (Thermo Fisher Scientific) in 1 ml cold cryopreservation medium (DMEM-GlutaMAX supplemented with 10% FBS and 10% DMSO), frozen at -80 °C in a freezing box and kept at -80 °C until use. On the day of the experiment, the samples were rapidly thawed in a water bath at 37 °C and tissues were washed twice with DMEM-GlutaMAX and twice with cold PBS. Tissues were then digested with 200 µl Versene solution (Thermo Fisher Scientific) for 20 min at 20 °C, and the cells were dissociated by pipetting several times. Several rounds of cell dissociation in DMEM-GlutaMAX were performed to get the maximal number of cells. Dissociated cells were then centrifuged at 3,000g for 5 min, and the cell pellet was washed with 1 ml of cold PBS and resuspended in 200 µl cold PBS.

Relative quantification of mGlu2 expression by TR-FRET

The TR-FRET protocol was performed as previously described⁵⁴. In brief, 10 µl of dissociated cells were added in a low-volume 96-well microplate (Revvity) and incubated with 10 µl DN10-d2 (25 nM), 10 µl DN1-Tb (25 nM) and 10 µl LY379268 (10 µM), to reach a total volume of 40 µl. Plates were incubated overnight at 22 °C and the sensitized acceptor emission (665 nm) was measured after excitation at 337 nm on the Pherastar FS plate-reader, in the optimal window as previously described⁶⁴. The resulting acceptor ratio window W2 (50–100 µs)/window W3 (1,200–1,600 µs) multiplied by 10⁴ was then plotted. In parallel, the total amount of proteins was determined using the BCA protein assay (Sigma-Aldrich). Absorbances were measured using the Infinite M200 system.

Animal experiment sample size determination, randomization and blinding

The sample size was determined through previous experience for the neurodevelopmental model⁶⁵; through power calculations using experimentally identified s.d. values and anticipated meaningful effect sizes for the genetic model⁶⁶; and using the free application developed by Data'Stat for the *in vivo* cerebral quantification (<http://appsonline.idele.fr/CalculEffectif/>). Randomization principle was used to assign experimental mice to treatment groups to avoid bias and spurious conclusions in all of the animal experiments⁶⁷. In the neurodevelopmental model, all pregnant female mice (Janvier Labs) were not reused to generate new litters. At weaning, each mouse was labelled with a unique ear tag. Within a cage, mice were randomly assigned to the different treatments tested. Thus, mice from different litters received the same treatment for a given cohort. Investigators were blinded to all of the experimental conditions whenever possible during data collection and they were blinded during data analysis. Further details are provided in the Reporting summary.

Statistical analyses

Data are expressed as the mean ± s.d. unless notified otherwise in the figure legend. The main experimental findings are representative of at least two independently performed experiments. The distribution of data in each set of experiments was initially analysed using Shapiro-Wilk's normality test using GraphPad Prism v.10.4.2 (GraphPad software). When datasets were normally distributed, parametric tests were performed: one-way ANOVA or Brown-Forsythe and Welch followed by post hoc Dunnett's multiple-comparison test. Behavioural analysis using GluNI-KD mice was analysed using two- or three-way ANOVA with or without repeated measures (rm-MANOVA and MANOVA) where necessary with further post hoc analysis (Tukey's HSD test).

Article

When datasets were not normally distributed, non-parametric Kruskal-Wallis tests were used followed by a Dunn's post hoc analysis. $P < 0.05$ was defined as a significant difference for all statistical analyses. Statistical analyses were performed with GraphPad Prism v.10.4.2 or TIBCO Statistica (v.14.0.0.15, TIBCO).

Reporting summary

Further information on research design is available in the Nature Portfolio Reporting Summary linked to this article.

Data availability

Protocols are provided with this paper. All other requests for materials will be promptly reviewed by the corresponding authors to determine whether they are subject to intellectual property. Source data are provided with this paper.

51. Sargin, D. et al. CREB regulates spine density of lateral amygdala neurons: implications for memory allocation. *Front. Behav. Neurosci.* **7**, 209 (2013).
52. Silva, A. J. et al. Mutant mice and neuroscience: recommendations concerning genetic background. *Neuron* **19**, 755–759 (1997).
53. Doumazane, E. et al. A new approach to analyze cell surface protein complexes reveals specific heterodimeric metabotropic glutamate receptors. *FASEB J.* **25**, 66–77 (2011).
54. Meng, J. et al. Nanobody-based sensors reveal a high proportion of mGlu heterodimers in the brain. *Nat. Chem. Biol.* **18**, 894–903 (2022).
55. Pais de Barros, J.-P. et al. Quantitative lipopolysaccharide analysis using HPLC/MS/MS and its combination with the limulus amebocyte lysate assay. *J. Lipid Res.* **56**, 1363–1369 (2015).
56. Larsen, P. P. et al. Association of lipopolysaccharide-type endotoxins with retinal neurodegeneration: the Alienor study. *Ophthalmol. Sci.* **5**, 100610 (2025).
57. Franklin, K. B. J. & Paxinos, G. *The Mouse Brain in Stereotaxic Coordinates, Compact—3rd Edition* (Elsevier, 2008); www.elsevier.com/books/the-mouse-brain-in-stereotaxic-coordinates-compact/franklin/978-0-12-374244-5.
58. Lipina, T. V., Zai, C., Hlousek, D., Roder, J. C. & Wong, A. H. C. Maternal immune activation during gestation interacts with Disc1 point mutation to exacerbate schizophrenia-related behaviors in mice. *J. Neurosci.* **33**, 7654–7666 (2013).
59. Lipina, T., Labrie, V., Weiner, I. & Roder, J. Modulators of the glycine site on NMDA receptors, D-serine and ALX 5407, display similar beneficial effects to clozapine in mouse models of schizophrenia. *Psychopharmacology* **179**, 54–67 (2005).
60. Paylor, R., Spencer, C. M., Yuva-Paylor, L. A. & Pieke-Dahl, S. The use of behavioral test batteries, II: effect of test interval. *Physiol. Behav.* **87**, 95–102 (2006).
61. Chen, Y. et al. Restoring striatal WAVE-1 improves maze exploration performance of GluN1 knockdown mice. *PLoS ONE* **13**, e0199341 (2018).
62. Xie, G. et al. Forward genetic screen of mouse reveals dominant missense mutation in the P/Q-type voltage-dependent calcium channel, CACNA1A. *Genes Brain Behav.* **6**, 717–727 (2007).
63. Amir, S., Brown, Z. W., Amit, Z. & Ornstein, K. Body pinch induces long lasting cataleptic like immobility in mice: behavioral characterization and the effect of naloxone. *Life Sci.* **28**, 1189–1194 (1981).
64. Scholler, P. et al. HTS-compatible FRET-based conformational sensors clarify membrane receptor activation. *Nat. Chem. Biol.* **13**, 372–380 (2017).
65. Berthoux, C. et al. Early 5-HT6 receptor blockade prevents symptom onset in a model of adolescent cannabis abuse. *EMBO Mol. Med.* **12**, e10605 (2020).
66. Krzywinski, M. & Altman, N. Power and sample size. *Nat. Methods* **10**, 1139–1140 (2013).
67. Hirst, J. A. et al. The need for randomization in animal trials: an overview of systematic reviews. *PLoS ONE* **9**, e98856 (2014).

Acknowledgements We thank P. Barbe, U. Alenda, R. Perrin, V. Pereira, L. Devel and P. Mollard for their experimental support and advice; W. Horsfall for genotyping GluN1-KD mouse line and S. Bauche and N. Boucharel for their help in nanobody production; the members of the Arpège facility at the Institut de Génomique Fonctionnelle, RAM-iExplore, IPAM and the DiviOomics facility at University of Bourgogne (Dijon, France) for providing facilities and technical support; and the staff at Revvity for their support in providing reagents. P.R., J.K., J.-P.P., F.V., C.B. and P.M. were supported by the Centre National de la Recherche Scientifique (CNRS), the University of Montpellier and the Institut National de la Santé et de la Recherche Médicale (INSERM). P.R. was supported by the French National Research Agency (ANR-15-CE18-0020-01, ANR-20-CE18-0011-02 and ANR-22-CE18-0003), Fondation pour la Recherche Médicale (EQU202303016470 and prematurity program PMT202407019488) and the transfer of Technology Agency SaTT AxLR Occitanie. J.-P.P. was supported by the Fondation pour la Recherche Médicale (no. DEQ 20170336747 and PMT202206015633) and the LabEx MAblImprove (ANR-10-LABX-5301). M.O. and M.E.T. were supported by a PhD fellowship, and P.-A.L. by a post-doctoral fellowship from the LabEx MAblImprove (ANR-10-LABX-5301). A.S. and A.J.R. were supported by operating grants from Canadian Institutes of Health Research. IPAM and Montpellier RIO Imaging facilities are supported by the French National Research Agency (ANR-10-INBS-04 FBI and ANR-24-INBS-0005 FBI).

Author contributions M.O., A.R., T.L., P.-A.L., M.E.T., M.K., H.C., P.C., P.M., L.P., D.S., A.S., A.J.R., C.B., J.-P.P., J.K. and P.R. designed research. M.O., A.R., T.L., P.-A.L., M.E.T., M.K., H.C., P.P.-S., S.D., C.D., C.C., C.L., D.M. and F.V. performed research. M.O., A.R., T.L., P.-A.L., M.E.T., M.K., H.C., D.S., A.S., A.J.R., C.B., J.-P.P., J.K. and P.R. analysed the data. M.O., J.-P.P., J.K. and P.R. wrote the paper. All of the authors reviewed and edited the manuscript.

Competing interests The authors have related patents granted under patent numbers WO2016001417A1 (J.-P.P., P.C. and P.R.), WO2024003389A1 (J.-P.P., P.R., P.C., J.K., M.O., A.R. and C.B.) and WO2024003390A1 (J.-P.P., P.R., L.P., J.K., M.O. and M.T.). The other authors declare no competing interests.

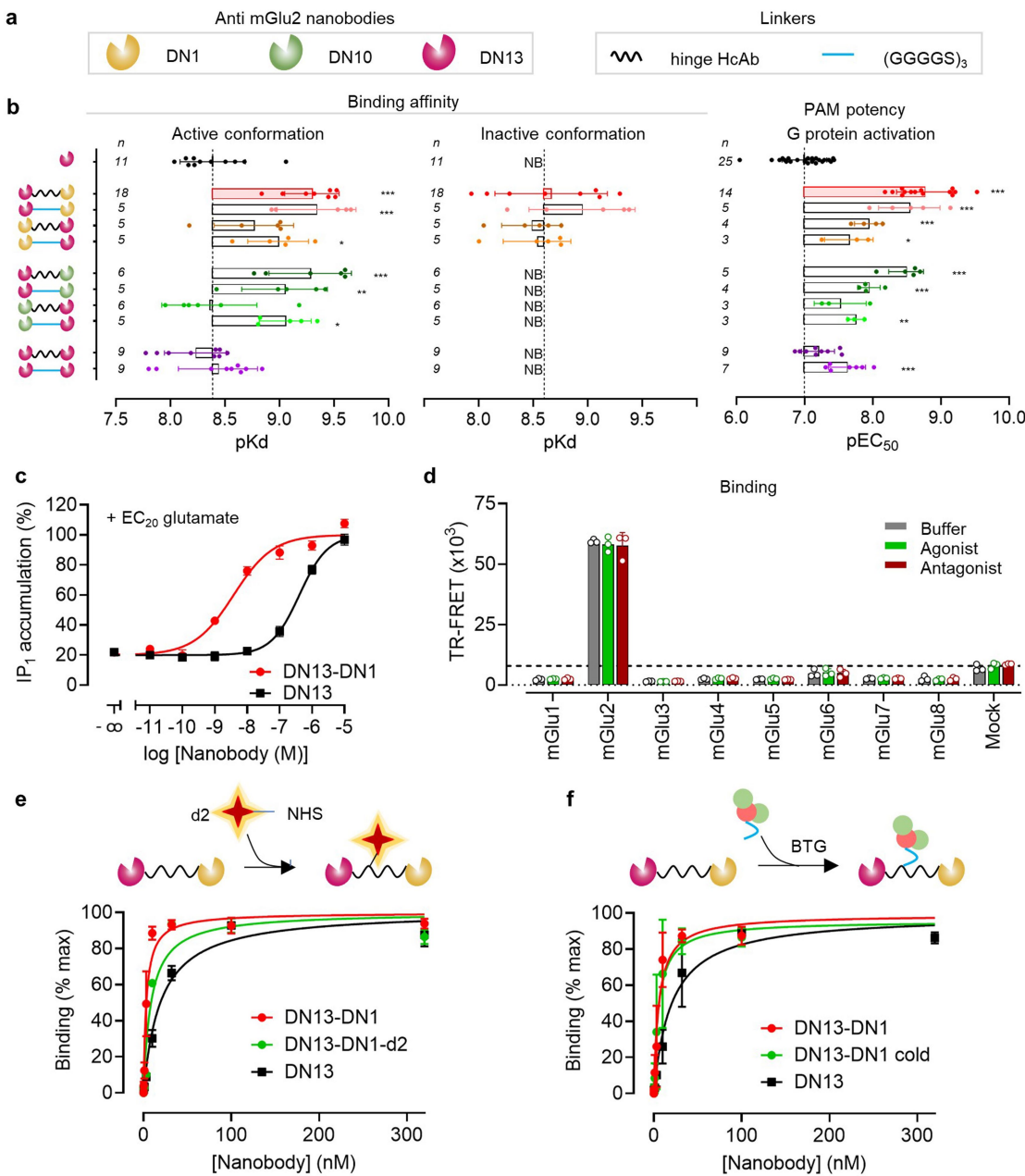
Additional information

Supplementary information The online version contains supplementary material available at <https://doi.org/10.1038/s41586-025-09265-8>.

Correspondence and requests for materials should be addressed to Jean-Philippe Pin, Julie Kniazeff or Philippe Rondard.

Peer review information *Nature* thanks Oliver Howes, Anne Messer, Alice Petty and the other, anonymous, reviewer(s) for their contribution to the peer review of this work. Peer reviewer reports are available.

Reprints and permissions information is available at <http://www.nature.com/reprints>.



Extended Data Fig. 1 | Comparison of mGlu₂ bivalent nanobodies.

a–b, Schematic representation of the indicated mGlu₂ nanobodies and linkers (*a*) used to generate a library of mGlu₂ bivalent nanobodies (*b*). **b**, Binding affinity on active (left) or inactive (centre) conformation of the mGlu₂ receptor and PAM potency (right) of all the bivalent nanobodies. Binding affinity for mGlu₂ receptor was determined in a FRET-based assay where the active and inactive conformations of the receptor were stabilized with saturating concentrations of LY379268 (1 μM) or LY341495 (1 μM), respectively. The dotted lines indicate the Kd values of DN13 binding (left panel) and of DN1 binding previously reported¹¹ (middle panel) and the bars highlight the difference from these reference values. The PAM potency was evaluated by measuring the accumulation of IP₁ in the presence of an EC₂₀ concentration of LY379268 (0.6 nM). Each data point represents the mean ± SD of the indicated number (n) of independent experiments performed in triplicates. Statistics are calculated using one-way ANOVA followed by a Dunnett multiple comparison test. *p < 0.05, **p < 0.01 and ***p < 0.001 compared to DN13. NB, no binding.

c, Potentiation of IP₁ accumulation induced by the indicated nanobodies in the presence of EC₂₀ of glutamate (5.42 μM). Data are mean ± SD of three individual experiments each performed in triplicates. **d**, Binding of DN13-DN1 on the different SNAP-mGlu receptor subtypes transfected in HEK293 cells in the presence of a saturating concentration of their respective agonists. Data are mean ± SD of three individual experiments each performed in triplicates.

e, Cartoon depicting DN13-DN1 labelling on native lysine residues using a N-hydroxysuccinimide fluorophore (d2-NHS). Saturation binding experiments for the labelled DN13-DN1-d2 on mGlu₂ expressing HEK293 cells, and comparison with nanobodies. Data are mean ± SD of four individual experiments each performed in triplicates. **f**, Cartoon depicting the bacterial transglutaminase (BTG) derivatization of DN13-DN1 using and CBz-Gln-Gly-Lys-OH peptide under controlled conditions to reach derivatization on a single lysine 121 in the linker HcAb as determined by mass spectrometry. Saturation binding experiments for the DN13-DN1 cold, derivatized as for the tritiated version, and comparison with the other unlabelled nanobodies. Values are a mean ± SD of two experiments each performed in quadruplicate. For details on statistics and p-values, see Source data.

presence of EC₂₀ of glutamate (5.42 μM). Data are mean ± SD of three individual experiments each performed in triplicates. **d**, Binding of DN13-DN1 on the different SNAP-mGlu receptor subtypes transfected in HEK293 cells in the presence of a saturating concentration of their respective agonists. Data are mean ± SD of three individual experiments each performed in triplicates.

e, Cartoon depicting DN13-DN1 labelling on native lysine residues using a N-hydroxysuccinimide fluorophore (d2-NHS). Saturation binding experiments for the labelled DN13-DN1-d2 on mGlu₂ expressing HEK293 cells, and comparison with nanobodies. Data are mean ± SD of four individual experiments each performed in triplicates. **f**, Cartoon depicting the bacterial transglutaminase (BTG) derivatization of DN13-DN1 using and CBz-Gln-Gly-Lys-OH peptide under controlled conditions to reach derivatization on a single lysine 121 in the linker HcAb as determined by mass spectrometry. Saturation binding experiments for the DN13-DN1 cold, derivatized as for the tritiated version, and comparison with the other unlabelled nanobodies. Values are a mean ± SD of two experiments each performed in quadruplicate. For details on statistics and p-values, see Source data.

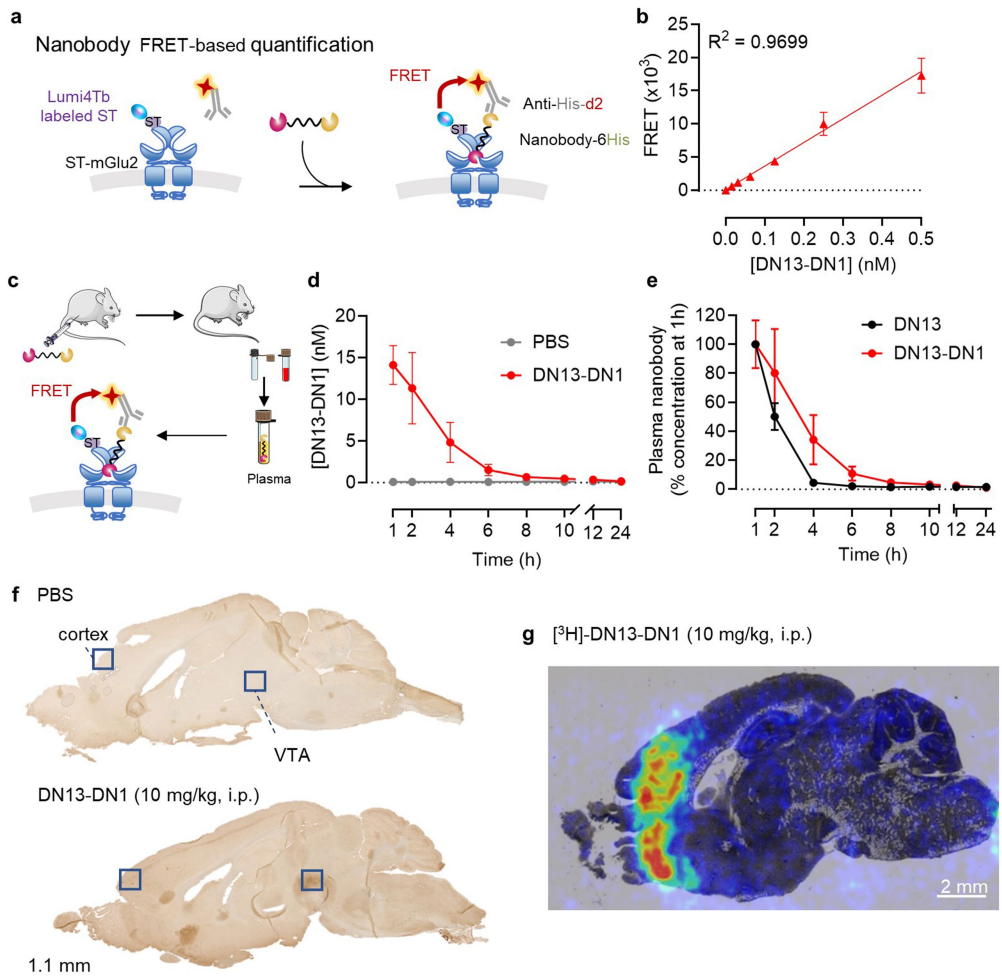
Article

Nanobody	Species	Human mGlu2		Rat mGlu2		Mouse mGlu2	
		(pKd)	State	Active*	Inactive**	Active*	Inactive**
DN1				8.80 ± 0.14	8.28 ± 0.12	8.37 ± 0.03	8.24 ± 0.02
DN13				8.39 ± 0.13	NB	8.39 ± 0.03	NB
DN13-DN1				9.69 ± 0.18	8.16 ± 0.07	9.30 ± 0.09	8.66 ± 0.52
DN13-Fc				8.56 ± 0.08	NB	8.31 ± 0.05	NB
						9.24 ± 0.01	8.18 ± 0.09
						8.35 ± 0.14	NB

Nanobody	Species	Human mGlu2		Rat mGlu2		Mouse mGlu2	
		(pEC ₅₀)	Agonist	LY379268	Glutamate	LY379268	Glutamate
DN1				Inactive	Inactive	Inactive	Inactive
DN13				7.38 ± 0.12	6.42 ± 0.10	7.00 ± 0.07	6.39 ± 0.07
DN13-DN1				8.71 ± 0.14	8.24 ± 0.27	8.75 ± 0.10	8.42 ± 0.16
DN13-Fc				7.52 ± 0.28	6.33 ± 0.30	7.07 ± 0.10	6.35 ± 0.06
						8.77 ± 0.42	8.18 ± 0.06
						7.57 ± 0.18	6.36 ± 0.07

Extended Data Fig. 2 | Pharmacological properties of DN1, DN13, DN13-DN1 and DN13-Fc on different mGlu₂ orthologues. **a**, Affinity of DN1, DN13, DN13-DN1 and DN13-Fc for various mGlu₂ orthologues. pKd values determined by binding experiments of the indicated nanobodies-derivatives on HEK293 cells expressing the indicated SNAP-mGlu₂ orthologue in the presence of a saturating concentration of the agonist LY379268 (1 μM) or the antagonist LY341495 (1 μM). Data are mean ± SD of three individual experiments each

performed in triplicates. **b**, PAM potency of DN1, DN13, DN13-DN1 and DN13-Fc for various mGlu₂ orthologues in the presence of an EC₂₀ of agonist. PAM potency (pEC₅₀) values determined in an IP₅ accumulation assay on cells expressing the indicated SNAP-mGlu₂ orthologue. Potentiation was assessed in the presence of EC₂₀ of LY379268 or EC₂₀ of glutamate. Data are mean ± SD of three individual experiments each performed in triplicates. For details on statistics and *p*-values, see Source data.

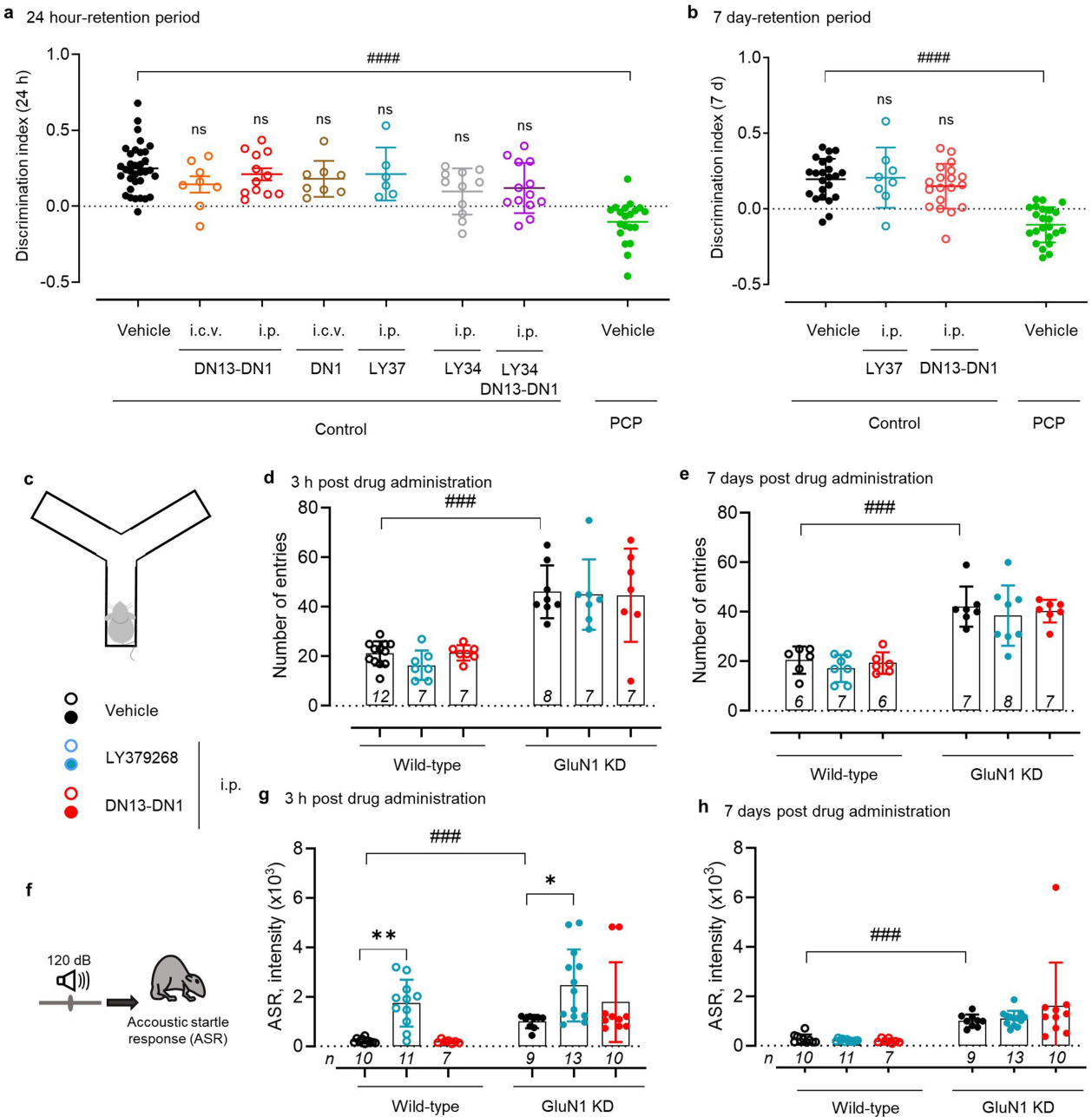


Extended Data Fig. 3 | Pharmacokinetics information on mGlu₂ nanobodies.

a, Schematic representation of the FRET-based quantification assay of 6His-tagged nanobodies. Cells expressing Lumi4Tb-labelled mGlu₂ receptors were incubated with a 6His-tagged nanobody in the presence of an anti-6His antibody coupled to the FRET acceptor d2. Under binding of the nanobody, FRET occurs. **b**, Linearity range of the assay for DN13-DN1 assessed using a known concentration of nanobody. **c**, Schematic representation of the nanobody quantification in the blood stream. After i.p. administration of the nanobody, the blood was collected over time and the plasma extracted. Samples were then used in the FRET-based quantification assay. **d**, Time course determination of DN13-DN1 (red) in the blood stream after i.p. administration of 10 mg/kg. Each data point is the mean \pm s.e.m. from three animals. **e**, Kinetics of DN13-DN1 (red) and DN13 (black) elimination from the blood stream.

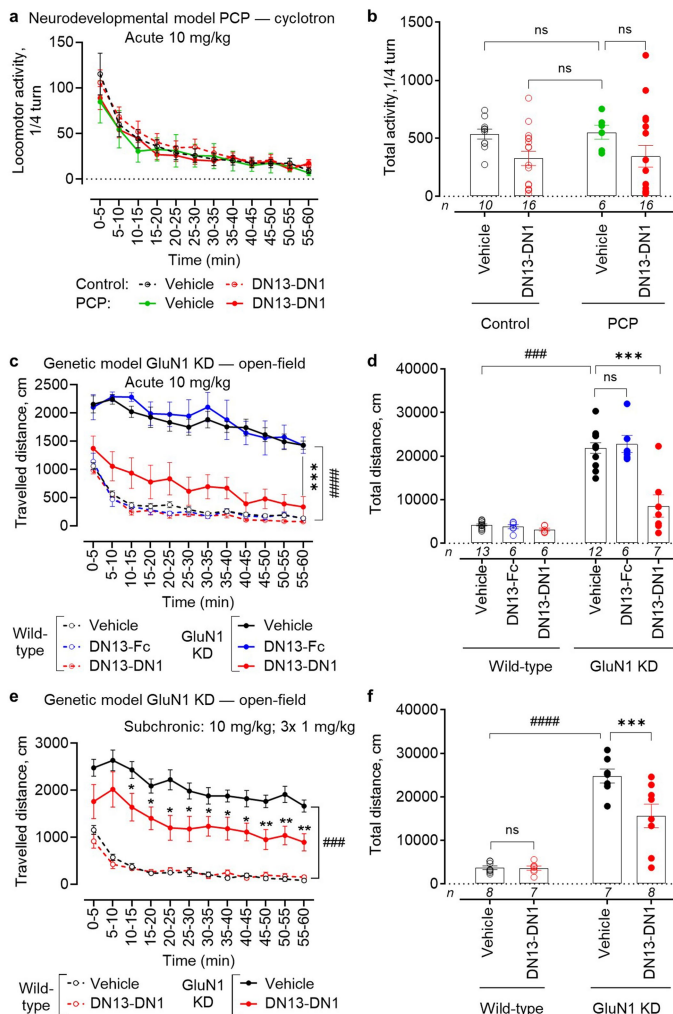
Each data point is the mean \pm s.e.m. from three animals. **f**, Representative immunohistochemical labelling with an anti-6His antibody of a sagittal slice from a mouse intraperitoneally administrated with either PBS (top) or 10 mg/kg of DN13-DN1 (bottom) and sacrificed 24 h after administration. DN13-DN1 contains a C-terminal 6His tag. Boxes indicate areas that were magnified in Fig. 1g. **g**, Representative slices of four technical replicates from two animals. VTA, ventral tegmental area. **g**, Autoradiographic signal in mouse brain slices 4 h after i.p. administration of [^{3}H]-DN13-DN1 at 10 mg/kg (3 μCi /mouse). Autoradiographic images were superimposed with transmission images of the same brain slices. Experiment performed in one animal. For details on statistics and *p*-values, see Source data. Panel **a** was partly generated using Servier Medical Art, provided by Servier, licensed under a CC 4.0.

Article

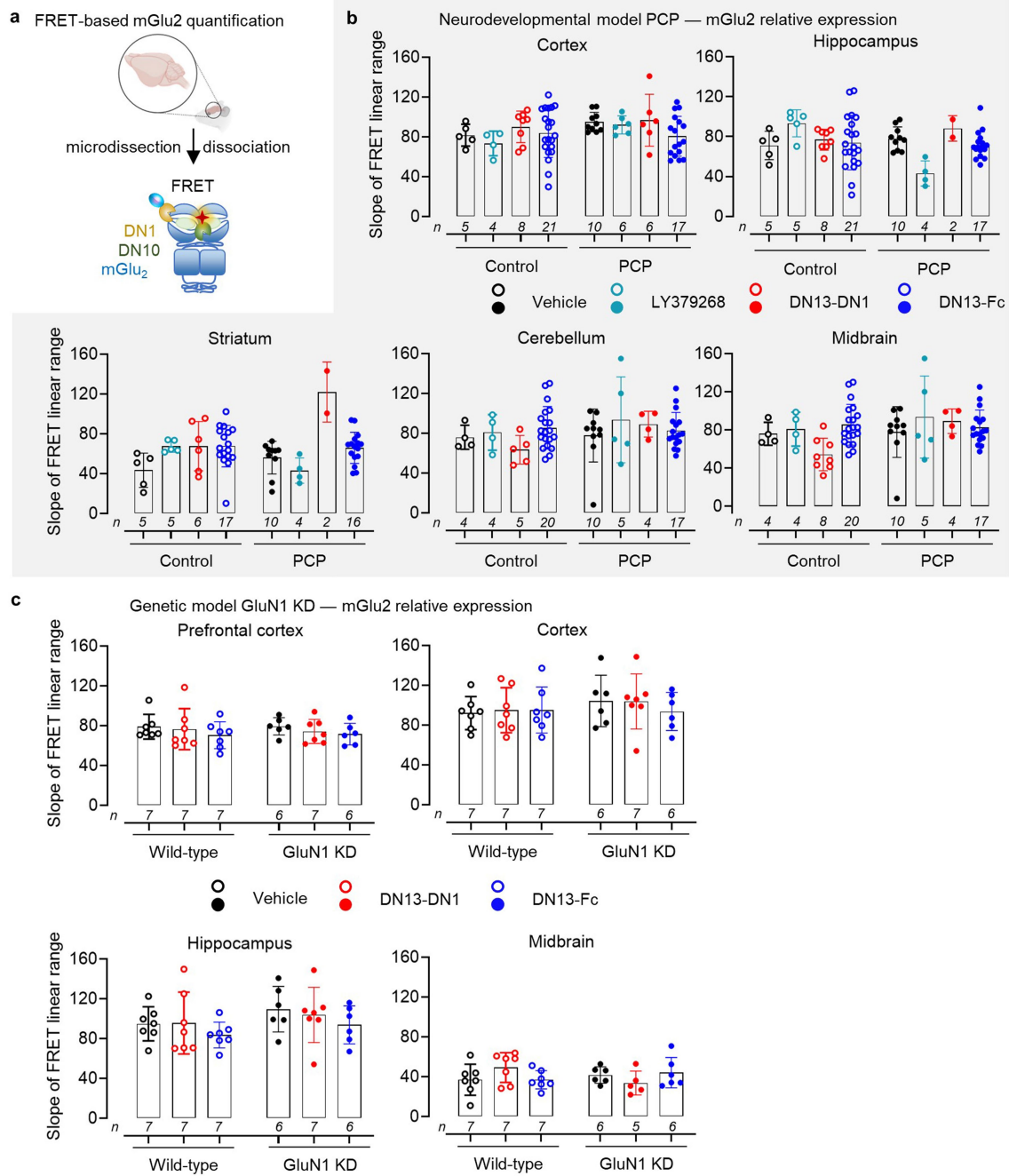


Extended Data Fig. 4 | Acute DN13-DN1 treatment does not alter discrimination index of control animal in NOR and ambulation or acoustic startle response in wild-type or GluN1 KD mice. **a, b**, Discrimination index in the NOR test performed 24 h (**a**) or 7 days (**b**) after the training session. **a**, Index obtained in control mice (black, $n = 34$) further treated with DN13-DN1 i.c.v. (orange, $n = 8$) or i.p. (red, $n = 12$), DN1 i.c.v. (brown, $n = 8$), mGlu₂ agonist (LY379268, blue, $n = 6$), mGlu₂ antagonist alone (LY341495, grey, $n = 11$) or with DN13-DN1 i.p. (purple, $n = 13$) and in PCP-treated mice (green, $n = 20$). **b**, Index obtained in control animals (black, $n = 23$) further treated with DN13-DN1 i.p. (red, $n = 19$) and LY379268 (blue, $n = 8$) and PCP-vehicle animals (green, $n = 23$). Bars represent means \pm SD. Statistics are calculated using one-way ANOVA. ns, non-significant and ##### $p < 0.0001$ compared to control mice. Note that vehicle- (black) and PCP-injected mice (green) are the same as those used in experiments illustrated in Fig. 2. **c–e**, Y-maze. Number of entries in Y-maze after acute injection at 3 h (**d**) and 7 days (**e**) as post-treatment period in vehicle (black), LY379268 (blue) and DN13-DN1 (red)-treated mice. Bars represent mean \pm SD. The number of animals is indicated at the bottom of the bar. #### $p < 0.0001$ in comparison with vehicle-treated WT; *** $p < 0.001$ in comparison with vehicle-treated GluN1 KD mice in two-way MANOVAs followed by a Tukey HDS test. **f–h**, Acoustic startle response (ASR) determined on vehicle (black), LY379268 (blue) and DN13-DN1-treated (red) mice assessed 3 h (**g**) or 7 days (**h**) after treatments. LY379268 (blue) increased startle response in both WT and GluN1 KD mice after 3 h of treatment but not seven days after treatment. Bars represent mean \pm SD. The number of animals is indicated above the X-axis. ### $p < 0.01$ in comparison with vehicle-treated WT mice; * $p < 0.05$ and ** $p < 0.01$ in comparison with vehicle-treated mice within each genotype in two-way MANOVAs followed by a Tukey HDS test. For details on statistics and p -values, see Source data.

acute injection at 3 h (**d**) and 7 days (**e**) as post-treatment period in vehicle (black), LY379268 (blue) and DN13-DN1 (red)-treated mice. Bars represent mean \pm SD. The number of animals is indicated at the bottom of the bar. #### $p < 0.0001$ in comparison with vehicle-treated WT; *** $p < 0.001$ in comparison with vehicle-treated GluN1 KD mice in two-way MANOVAs followed by a Tukey HDS test. **f–h**, Acoustic startle response (ASR) determined on vehicle (black), LY379268 (blue) and DN13-DN1-treated (red) mice assessed 3 h (**g**) or 7 days (**h**) after treatments. LY379268 (blue) increased startle response in both WT and GluN1 KD mice after 3 h of treatment but not seven days after treatment. Bars represent mean \pm SD. The number of animals is indicated above the X-axis. ### $p < 0.01$ in comparison with vehicle-treated WT mice; * $p < 0.05$ and ** $p < 0.01$ in comparison with vehicle-treated mice within each genotype in two-way MANOVAs followed by a Tukey HDS test. For details on statistics and p -values, see Source data.



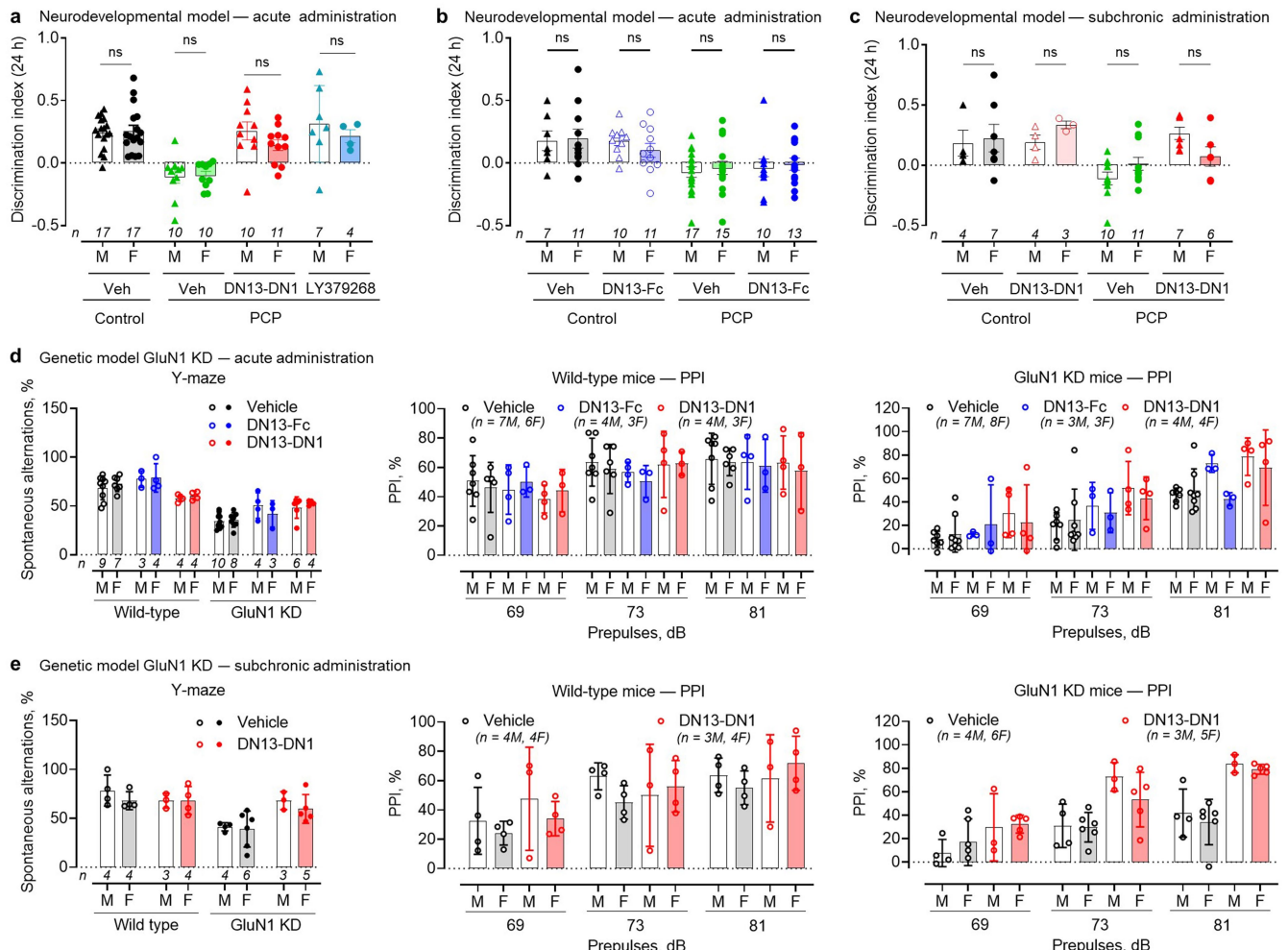
Extended Data Fig. 5 | Locomotor activity measured in the two mouse models after acute or subchronic treatment. **a–b**, DN13-DN1 acute treatment (red) does not modify the locomotor activity across 5-min bins (**a**) or total activity over 60 min (**b**) of control or PCP-treated mice, using a cyclotron. Data are presented as mean \pm s.e.m. (**a**) or mean \pm SD (**b**) and analysed using the one-way ANOVA followed by a Dunnett post-hoc analysis, ns: non-significant in comparison with vehicle-treated mice. **c–f**, Both DN13-DN1 acute (**c, d**) and subchronic (**e, f**) treatment decrease the hyperlocomotor activity of GluN1 KD mice assessed in an open-field using the travelled distance across 5-min bins (**c, e**) or total distance (**d, f**). Data are presented as mean \pm s.e.m. (**c, e**) or mean \pm SD (**d, f**). # $\#\#$ $p < 0.001$ and # $\#\#\#$ $p < 0.0001$ in comparison with vehicle-treated WT; ** $p < 0.001$ in comparison with vehicle-treated GluN1 KD mice; ns: non-significant; using two-way MANOVAs followed by a Tukey HDS test. The number of animals is indicated above the X-axis. For details on statistics and p -values, see Source data.



Extended Data Fig. 6 | mGlu₂ relative expression measured after acute treatment with DN13-DN1 in the two mouse models of schizophrenia.

a, Schematic representation of the FRET-based assay for quantification of mGlu₂ receptors expression using DN1 nanobody coupled to a donor (DN1-Tb) and DN10 coupled to an acceptor (DN10-d2). **b**, No significant differences were observed on the relative quantification of mGlu₂ receptors in the cortex, hippocampus, striatum, cerebellum and midbrain of control and PCP-treated mice injected with either LY379268 (1 mg/kg, light blue), DN13-DN1 (10 mg/kg, red), DN13-Fc (10 mg/kg, dark blue), or with vehicle (black). **c**, No variation in

the mGlu₂ relative expression was also observed between WT and GluN1 KD mice in the prefrontal cortex, cortex, hippocampus and midbrain, after an acute treatment with DN13-DN1 (10 mg/kg, red), DN13-Fc (10 mg/kg, blue) or with vehicle (black). The signal indicates the slope values of the relative FRET linear range in the quantification experiments. Data are presented as mean \pm SD and analysed using the one-way ANOVA followed by a Dunnett post-hoc analysis. The number of animals is indicated above the X-axis. For details on statistics and p-values, see Source data. Parts of panel **a** were created in Biorender. Lafon, P. (2025) <https://Biorender.com/w77j520>.



Extended Data Fig. 7 | Absence of sex-dependency of both acute and subchronic DN13-DN1 positive behavioural effect. Animals used in the experiments illustrated in Fig. 2c (a), Fig. 4b (b), Fig. 4c,d (d), Fig. 5b (c) and Fig. 5c,d (e) were separated according to their sex and analysed for potential sex difference. No significant differences were observed when comparing males (M) and females (F) for the neurodevelopmental model (a-c) and GluN1

KD mice (d,e), upon treatment with DN13-DN1 (acute or subchronic), DN13-Fc, LY379268 or vehicle. Statistics were calculated using unpaired Student's t-test or Mann-Whitney test (a-c) or three-way MANOVA (Y-maze) or three-way rm-MANOVA (PPI) followed by a Tukey HDS test (d-e), ns: non-significant. The number of animals is indicated above the X-axis. All data are mean ± SD. For details on statistics and p-values, see Source data.

Article

a

Treatments	WT		GluN1 KD	
	Male	Female	Male	Female
Acute administration (n = 60). Figure 3e-f				
Vehicle	27.5 ± 1.5 (n = 5)	20.6 ± 0.5 (n = 5)***	21.6 ± 0.3 (n = 4)###	20.0 ± 0.4 (n = 5)
LY379268	29.8 ± 0.6 (n = 6)	21.9 ± 0.5 (n = 5)	21.8 ± 0.3 (n = 7)	20.9 ± 0.7 (n = 6)
DN13-DN1	28.7 ± 1.1 (n = 3)	22.8 ± 0.9 (n = 4)	22.7 ± 0.3 (n = 5)	21.2 ± 0.8 (n = 5)
Acute administration (n = 56). Figure 4d				
Vehicle	29.2 ± 1.2 (n = 7)	23.3 ± 0.4 (n = 6)***	22.2 ± 0.4 (n = 7)###	20.9 ± 0.4 (n = 8)
DN13-Fc	28.4 ± 1.1 (n = 4)	21.9 ± 0.8 (n = 3)	23.1 ± 0.4 (n = 3)	21.4 ± 0.5 (n = 3)
DN13-DN1	31.7 ± 0.7 (n = 4)	22.8 ± 1.3 (n = 3)	22.8 ± 0.3 (n = 4)	20.9 ± 0.5 (n = 4)
Subchronic administration (n = 33). Figure 5d				
Vehicle	29.9 ± 2.5 (n = 4)	22.1 ± 0.8 (n = 4)***	20.9 ± 0.4 (n = 4)###	20.2 ± 0.2 (n = 6)
DN13-DN1	29.8 ± 0.5 (n = 3)	21.9 ± 0.4 (n = 4)	21.9 ± 0.4 (n = 3)	21.9 ± 0.7 (n = 5)

b

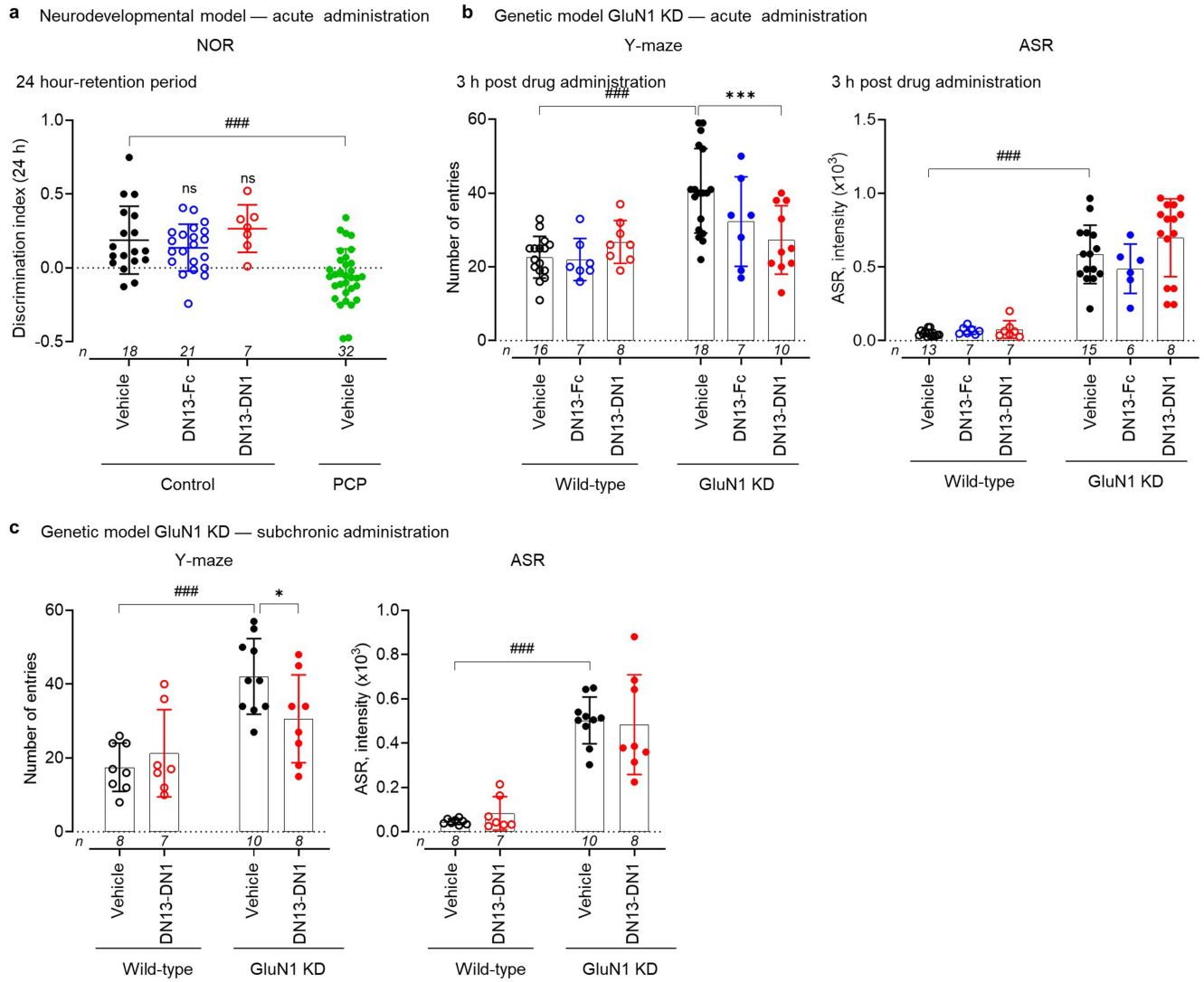
Body weight, g	PPI at 69 dB, %	PPI at 73 dB, %	PPI at 81 dB, %	ASR
Acute administration (n = 60). Figure 3e				
	R = 0.14; p = 0.25	R = 0.18; p = 0.19	R = 0.09; p = 0.49	R = -0.31; p < 0.05, *
Acute administration (n = 60). Figure 3f				
	R = 0.28; p = 0.42	R = 0.26; p = 0.06	R = 0.21; p = 0.11	R = -0.25; p < 0.05, *
Acute administration (n = 56). Figure 4d				
	R = 0.32; p = 0.31	R = 0.27; p = 0.12	R = 0.16; p = 0.25	R = -0.53; p < 0.001, ***
Subchronic administration (n = 33). Figure 5d				
	R = 0.33; p = 0.07	R = 0.28; p = 0.11	R = 0.22; p = 0.23	R = -0.52; p < 0.01, **

c

Test	Parameter	Vehicle n = 7 (3F/4M)	DN13-DN1 n = 7 (3F/4M)
Inclined platform	Latency, sec	27.1 ± 2.5	26.1 ± 2.6
Rotarod	Latency, sec	87.6 ± 3.9	85.0 ± 2.6
Pinch-induced catalepsy	Immobility, sec	43.6 ± 5.3	47.0 ± 3.0

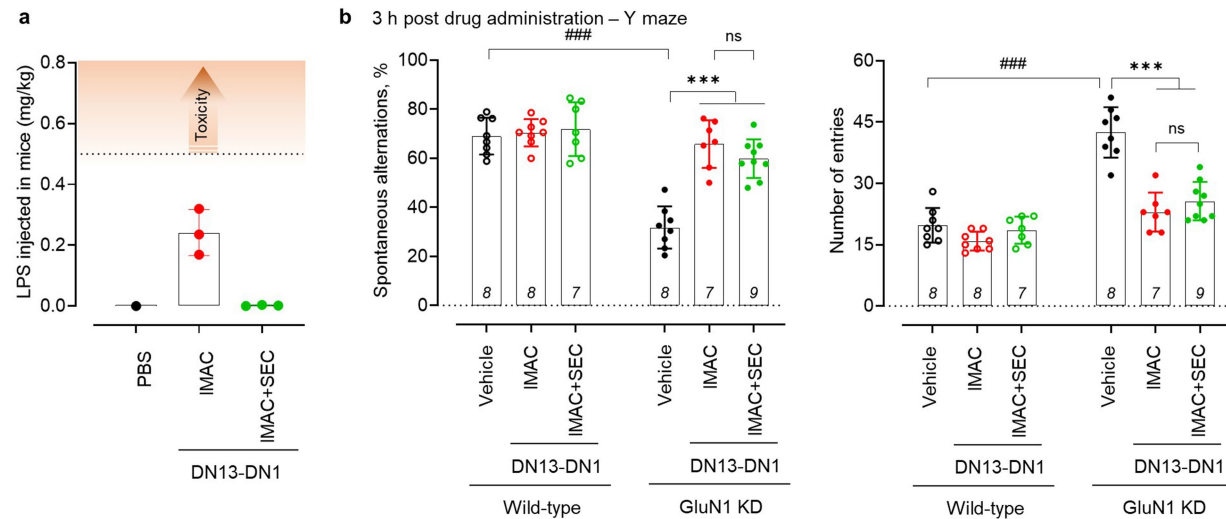
Extended Data Fig. 8 | Absence of body weight influence on PPI results and absence of DN13-DN1 effect on locomotion and cataleptic behaviour in control mice. **a**, Recapitulation of body weight of animals used in experiments illustrated in Figs. 3, 4 and 5. ***p < 0.001 in comparison with PBS-treated males within genotype; ###p < 0.001 in comparison with PBS-treated WT mice. **b**, Pearson's correlations among body weight, percentage of pre-pulse inhibition (PPI, %) at various pre-pulses and acoustic startle response (ASR) across all experiments. No correlation was found between body weight and PPI, however, a negative association was found between body weight and ASR,

attributed to the increased startle response in GluN1 KD mice with lower body weight. **c**, Effects of DN13-DN1 acute treatment (10 mg/kg) on motor coordination and balance (inclined platform and rotarod), and cataleptic behaviour (pinch-induced catalepsy) in WT mice. Data are presented as mean ± s.e.m. and analysed by a two-way MANOVA (**a**) or three-way MANOVA (**c**) followed by a Tukey HDS test and Pearson's correlation (**b**). The numbers of animals are indicated in the panels. For more details on statistics, see Source data.



Extended Data Fig. 9 | Acute DN13-Fc and subchronic DN13-DN1 treatment do not alter discrimination index of control animals in NOR and ambulation or acoustic startle response in wild-type or GluN1 KD mice. **a**, Discrimination index in the NOR test performed 24 h after the training session. DN13-DN1 and DN13-Fc were administered 3 h before the training session, respectively. Neither DN13-DN1 (10 mg/kg, i.p., red) nor DN13-Fc (10 mg/kg, i.p., blue) modified the discrimination score compared to vehicle treated animal (black). Bars represent means \pm SD. Statistics were calculated using Kruskal-Wallis test followed by a Dunn's multiple comparison test, ns: non-significant and $### p < 0.001$ compared to control mice. Note that vehicle- (black) and PCP-injected mice (green) are the same as those used in experiments illustrated in

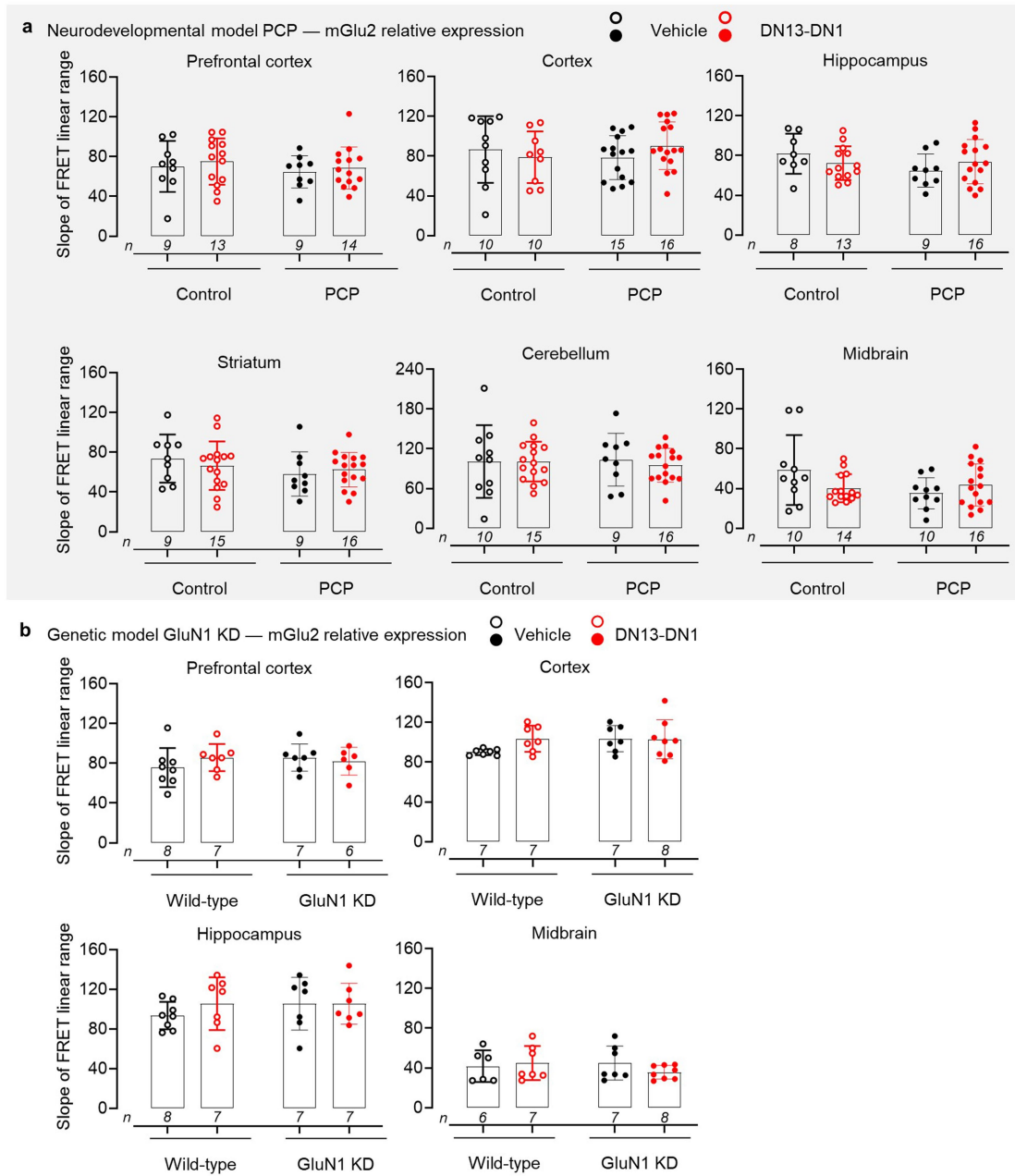
Fig. 5b,b,c. Effect of acute administration of DN13-Fc (10 mg/kg, i.p., blue) or DN13-DN1 (10 mg/kg, i.p., red). **Left panel.** Number of entries in Y-maze: DN13-DN1 (red) but not DN13-Fc (blue) reduced ambulation in Y-maze. **Right panel.** Acoustic startle response (ASR) was not altered by treatment. Bars represent mean \pm SD. **c**, Effect of subchronic administration of DN13-DN1 (10 mg/kg, 3 \times 1 mg/kg, i.p., red) on number of entries in Y-maze (**left panel**) or ASR (**right panel**). Bars represent mean \pm SD. In **b,c**, $### p < 0.01$ in comparison with vehicle-treated WT mice; $** p < 0.01$ in comparison with vehicle-treated mice within each genotype in two-way MANOVA followed by a Tukey HDS test. In **a,b,c** the numbers of animals are indicated in the panels. For details on statistics and *p*-values see Source data.



Extended Data Fig. 10 | Low LPS contamination of DN13-DN1 is not responsible for nanobody brain-penetration or behavioural effect.

a, Evaluation of LPS amount injected into animals during DN13-DN1 administration. The content of LPS in each nanobody sample was assessed by mass spectrometry ($n = 3$ biological samples). Along DN13-DN1 purified in the standard protocol (Immobilized-metal affinity chromatography – IMAC) administration, around 0.25 mg/kg LPS are injected into animals which is below the threshold reported to induce toxicity (0.5 mg/kg). A further size exclusion chromatography (SEC) purification step reduces this amount to 0.002 mg/kg. Results in DN13-DN1 nanobody with almost no endotoxin

(below 0.19 μ g/mg nanobody) still have an acute effect in the genetic mouse model of schizophrenia. **b**, Y-maze. Percentage of spontaneous alternations and number of entries 3 h after the acute injection of 10 mg/kg (i.p.) of DN13-DN1 either purified in one-step IMAC or purified in two steps IMAC followed by SEC. No difference was observed between DN13-DN1 samples, and both samples significantly corrected the working memory deficit in GluN1 KD mice. Bars represent mean \pm SD. ### $p < 0.001$ in comparison with vehicle-treated WT mice; *** $p < 0.001$ in comparison with vehicle-treated GluN1 KD mice in two-way MANOVA followed by a Tukey HDS test. The numbers of animals are indicated in the panels. For details on statistics and p -values, see Source data.



Extended Data Fig. 11 | mGlu₂ relative expression measured after subchronic treatment with DN13-DN1 in the two mouse models of schizophrenia. **a**, No significant differences were observed on the relative quantification of mGlu₂ receptors in the prefrontal cortex, cortex, hippocampus, striatum, cerebellum and midbrain of control and PCP-treated mice treated with DN13-DN1 (red) or vehicle (black) subchronic protocol detailed in Fig. 5a (10 mg/kg, 3 × 1 mg/kg). **b**, No variation in the mGlu₂ relative expression was

also observed between subchronic administration of DN13-DN1 (10 mg/kg, 3 × 1 mg/kg, red) or vehicle (black) in both WT and GluN1 KD mice. The signal indicates the slope values of the relative FRET linear range in the quantification experiments. Data are presented as mean ± SD and analysed using the one-way ANOVA followed by a Dunnett post-hoc analysis. The number of animals is indicated above the X-axis. For details on statistics and *p*-values, see Source data.

Reporting Summary

Nature Portfolio wishes to improve the reproducibility of the work that we publish. This form provides structure for consistency and transparency in reporting. For further information on Nature Portfolio policies, see our [Editorial Policies](#) and the [Editorial Policy Checklist](#).

Statistics

For all statistical analyses, confirm that the following items are present in the figure legend, table legend, main text, or Methods section.

n/a Confirmed

- The exact sample size (n) for each experimental group/condition, given as a discrete number and unit of measurement
- A statement on whether measurements were taken from distinct samples or whether the same sample was measured repeatedly
- The statistical test(s) used AND whether they are one- or two-sided
Only common tests should be described solely by name; describe more complex techniques in the Methods section.
- A description of all covariates tested
- A description of any assumptions or corrections, such as tests of normality and adjustment for multiple comparisons
- A full description of the statistical parameters including central tendency (e.g. means) or other basic estimates (e.g. regression coefficient) AND variation (e.g. standard deviation) or associated estimates of uncertainty (e.g. confidence intervals)
- For null hypothesis testing, the test statistic (e.g. F , t , r) with confidence intervals, effect sizes, degrees of freedom and P value noted
Give P values as exact values whenever suitable.
- For Bayesian analysis, information on the choice of priors and Markov chain Monte Carlo settings
- For hierarchical and complex designs, identification of the appropriate level for tests and full reporting of outcomes
- Estimates of effect sizes (e.g. Cohen's d , Pearson's r), indicating how they were calculated

Our web collection on [statistics for biologists](#) contains articles on many of the points above.

Software and code

Policy information about [availability of computer code](#)

Data collection

All FRET measurements (TR-FRET and HTRF) were acquired using PHERAstar control software version 5.41 (BMG LabTech). Image acquisition was done using ZEN slidescan Zen 2.3 Lite (Zeiss). Images were processed and exported as TIFF using ZEN 3.2 blue edition (Zeiss). Beta-radioactivity was quantified using QuantaSmart program (QuantaSmart program: version 5.2 on Windows® 10, 64-bit for the Tri-Carb Liquid Scintillation Analyzer series of instruments) and imaged on BETA-Imager using BetaAcquisition software version 9.4.12. 219 which seamlessly control the entire system and its modules, and manage the imaging experiments. For NOR experiments, the animals were videotracker using Ethovision software XT 13.0 (Noldus) or Logitech capture : 2.08.11 and blind analysis was done using a virtual timer (xntimer 1.12.0.0). For Y-maze, behavioral results were collected semi-automatically using video-tracking software (Biobserve Viewer2.0 tracking software). PPI data were collected using SR-Lab Analysis software 6300-0000-Y.

Data analysis

Data were plotted and statistically analyzed using Prism 10.4.2 (Graphpad software) except for Y-maze and PPI data that were statistically analyzed using TIBCO Statistica 14.0.0.15 software.

For manuscripts utilizing custom algorithms or software that are central to the research but not yet described in published literature, software must be made available to editors and reviewers. We strongly encourage code deposition in a community repository (e.g. GitHub). See the Nature Portfolio [guidelines for submitting code & software](#) for further information.

Data

Policy information about [availability of data](#)

All manuscripts must include a [data availability statement](#). This statement should provide the following information, where applicable:

- Accession codes, unique identifiers, or web links for publicly available datasets
- A description of any restrictions on data availability
- For clinical datasets or third party data, please ensure that the statement adheres to our [policy](#)

Source data and protocols are provided with this paper. All other requests for materials will be promptly reviewed by the corresponding authors to determine whether they are subject to intellectual property.

Research involving human participants, their data, or biological material

Policy information about studies with [human participants or human data](#). See also policy information about [sex, gender \(identity/presentation\), and sexual orientation](#) and [race, ethnicity and racism](#).

Reporting on sex and gender [No involvement of human participants, their data or biological material](#)

Reporting on race, ethnicity, or other socially relevant groupings [No involvement of human participants, their data or biological material](#)

Population characteristics [No involvement of human participants, their data or biological material](#)

Recruitment [No involvement of human participants, their data or biological material](#)

Ethics oversight [No involvement of human participants, their data or biological material](#)

Note that full information on the approval of the study protocol must also be provided in the manuscript.

Field-specific reporting

Please select the one below that is the best fit for your research. If you are not sure, read the appropriate sections before making your selection.

Life sciences Behavioural & social sciences Ecological, evolutionary & environmental sciences

For a reference copy of the document with all sections, see nature.com/documents/nr-reporting-summary-flat.pdf

Life sciences study design

All studies must disclose on these points even when the disclosure is negative.

Sample size [Pharmacology](#): Sample size for each experiments were determined based on standards for experimental cell biology, with a minimum of n = 3 biological independent replicates with sufficient reproducibility. All the presented data are mean ± SEM or representative results for at least three experiments performed independently in triplicate or quadruplicate. Information on the number of replicates and independent experiments that were performed for each measurement is provided in the manuscript.

[Animal experiments](#):

[Neurodevelopment model](#): The sample size for behavioral studies using the PCP pharmacological model of schizophrenia was based on previous experiments carried-out in P. Marin's team on this same model (Rogliardo et al., in preparation) and on the model of chronic consumption of THC during adolescence (Berthoux et al, EMBO Molecular Medicine, 2020, doi: 10.1525/emmm.201910605).

[Genetic model](#): Group sizes were determined through power calculations, utilizing experimentally identified standard deviations and anticipated meaningful effect size, as recommended (Krywinski, M., Altman, N. Power and sample size. Nat Methods, 2013, 10, 1139–1140, doi: 10.1038/nmeth.2738).

[Radioactivity experiments](#): Sample size were determined thanks to a free application developed by Data'Stat (<http://appsonline.ideal.fr/CalculEffectif/>)

Data exclusions For *in vitro* experiments, some individual outliers were excluded from the analysis.
For NOR behavioral testing, mice with total time exploration of less than 3 sec in the test session were excluded.
For mGlu2 quantification some outliers and some samples below the limit of detection were excluded.

Replication Number of independent experiments and replicates are indicated in the legends to the figures.

Randomization Randomization principle was used to assign experimental mice to treatment groups to avoid bias and spurious conclusions in all animal experiments (Hirst JA., Howick J., Aronson JK., Roberts N., Perera R., Koshiaris C., Heneghan C. The need for randomization in animal trials: an overview of systematic reviews. PLoS One, 2014, 9(6):e98856, doi: 10.1371/journal.pone.0098856).
More specifically for neurodevelopmental model, to avoid any bias in the treatment attribution: all pregnant females were ordered from Janvier Labs, the females were not reused to generate new litters, at weaning, each mouse was labelled with a unique ear tag, within a cage, animals were randomly assigned to the different treatments tested. Thus, animals from different litters received the same treatment for a

given cohort.
For radioactivity experiments, animals were allocated to groups using a computerized randomization procedure.

Blinding

For all animal experiment (NOR, Y-maze, PPI, locomotion, radioactivity measurement, blood quantification, mGlu2 expression quantification) investigators were blind to all the experimental conditions whenever it was possible during data collection and they were blind during data analysis. This was notably done by assigning mice a digital identifier (code) and division of tasks (genotyping, treatment delivery, phenotyping and data analysis) between group members as recommended (Hirst et al., 2014). Genotyping was difficult to blind since Grin1 knockdown mice express pronounced hyperactivity and stereotypy.
For pharmacology experiments, investigators were aware of the samples identity.

Reporting for specific materials, systems and methods

We require information from authors about some types of materials, experimental systems and methods used in many studies. Here, indicate whether each material, system or method listed is relevant to your study. If you are not sure if a list item applies to your research, read the appropriate section before selecting a response.

Materials & experimental systems		Methods
n/a	Involved in the study	n/a Involved in the study
<input type="checkbox"/>	<input checked="" type="checkbox"/> Antibodies	<input checked="" type="checkbox"/> ChIP-seq
<input type="checkbox"/>	<input checked="" type="checkbox"/> Eukaryotic cell lines	<input checked="" type="checkbox"/> Flow cytometry
<input checked="" type="checkbox"/>	<input type="checkbox"/> Palaeontology and archaeology	<input checked="" type="checkbox"/> MRI-based neuroimaging
<input type="checkbox"/>	<input checked="" type="checkbox"/> Animals and other organisms	
<input checked="" type="checkbox"/>	<input type="checkbox"/> Clinical data	
<input checked="" type="checkbox"/>	<input type="checkbox"/> Dual use research of concern	
<input checked="" type="checkbox"/>	<input type="checkbox"/> Plants	

Antibodies

Antibodies used	Home made nanobodies: DN1, DN10, DN13 and the various bivalent combinations described in the article (several production were necessary to perform the behavioral experiments. All lots were pharmacologically validated prior to their use in animals). MAb Anti 6HIS-d2 (Revvity, #61HISDLF, lot :34B, and 40A) 6x-His Tag Recombinant Rabbit Monoclonal Antibody (Life technologie, clone RM146, #MA5-33032 , lot: YE3940631 and YB3826421) biotinylated goat anti-rabbit IgG (Vector Laboratories, #BA-1000-1.5, lot: ZH0106 for the antibody; ZJ0214 and ZJ0909 for DAB kit)
Validation	The specificity of DN1, DN10 and DN13 was previously reported (Scholler et al. Nat Comm (2017), dpo: 10.1038/s41467-017-01489-1). The specificity of DN13-DN1 was assessed in this study (Figure 1e and Extended data 1d). Commercial primary antibodies used in this study are widely used and have been validated by the respective manufacturer: Mab Anti 6His-d2 : https://resources.revvity.com/pdfs/rvtv_ls_manual_61HISDLF-61HISDLA-61HISDLB.pdf 6x-His Tag Recombinant Rabbit Monoclonal Antibody : https://www.thermofisher.com/order/genome-database/dataSheetPdf?producttype=antibody&productsuite=antibody_primary&productId=MA5-33032&version=Local .

Eukaryotic cell lines

Policy information about [cell lines and Sex and Gender in Research](#)

Cell line source(s)	HEK293 cells (ATCC, CRL-1573), HEK293F cells (Expi293™ Expression System Kit, ThermoFischer scientific, #A14635).
Authentication	HEK293 cell line was obtained from ATCC and HEK293F cell line from ThermoFisher scientific and used without further authentication.
Mycoplasma contamination	Putative Mycoplasma contamination was assessed monthly and no contamination was reported.
Commonly misidentified lines (See ICLAC register)	No commonly misidentified cell lines were used in this study.

Animals and other research organisms

Policy information about [studies involving animals; ARRIVE guidelines](#) recommended for reporting animal research, and [Sex and Gender in Research](#)

Laboratory animals	C57BL/6J mice either wild-type or GluN1 KD were used. For NOR behavioral experiments, pups were treated at P7, P9 and P11 and the behavioural was performed at P60 or P67.
Wild animals	The study did not involve wild animals.
Reporting on sex	Sex was not considered in the initial study design and gender analysis was performed (Extended data 7).

Field-collected samples	The study did not involve samples collected from field.
Ethics oversight	Animal care and surgical procedures were performed according to the Directive 2010/63/EU of the European Parliament, which had been approved by the Ministry of Agriculture, France. The project was approved by the French National Ethics Committee for Animal Experimentation (CEEA) under the number APAFIS #36241-2022032518526906 v4 (for PCP procedure), APAFIS#4111-2016021613253432 v5 (for tritiated nanobodies) and APAFIS #31981-2021060423426200 v3 (for nanobody pharmacokinetics in blood). Behavioural pharmacology in GluN1 KD mice was approved by the Faculty of Medicine and Pharmacy Animal Care Committee at the University of Toronto in accordance with Canadian Council on Animal Care (CCAC) guidelines. All experiments were performed in accordance with relevant named guidelines and regulations.

Note that full information on the approval of the study protocol must also be provided in the manuscript.

Plants

Seed stocks	No plants were used
Novel plant genotypes	No plants were used
Authentication	No plants were used